



# 1 Modelling snowpack on ice surfaces with the ORCHIDEE land surface 2 model: Application to the Greenland ice sheet

3 Sylvie Charbit<sup>1</sup>, Christophe Dumas<sup>1</sup>, Fabienne Maignan<sup>1</sup>, Catherine Ottlé<sup>1</sup>, Nina Raoult<sup>2</sup>,  
4 Xavier Fettweis<sup>3</sup>

5 <sup>1</sup>Laboratoire des Sciences du Climat et de l'Environnement, LSCE/IPSL, UMR 8212 CEA-CNRS-UVSQ,  
6 Université Paris-Saclay, 91191, Gif-sur-Yvette, France.

7 <sup>2</sup>Department of Mathematics and Statistics, Faculty of Environment, Science and Economy, University of Exeter,  
8 Laver Building, North Park Road, Exeter, EX4 4QE, United Kingdom.

9 <sup>3</sup>Laboratory of Climatology, Department of Geography, SPHERES, University of Liège, Liège, Belgium.

10 *Correspondence to:* Sylvie Charbit (sylvie.charbit@lsce.ipsl.fr)

11 **Abstract.** Current climate warming is accelerating mass loss from glaciers and ice sheets. In Greenland, the rates  
12 of mass changes are now dominated by changes in surface mass balance (SMB) due to increased surface melting.  
13 To improve the future sea-level rise projections, it is therefore critical to have an accurate estimate of the SMB,  
14 which depends on the representation of the processes occurring within the snowpack. The snow scheme (ES)  
15 implemented in the land surface model ORCHIDEE has not yet been adapted to ice-covered areas. Here, we  
16 present the preliminary developments we made to apply the ES model to glaciers and ice sheets. Our analysis  
17 mainly concerns the model's ability to represent ablation-related processes. At the regional scale, our results are  
18 compared to the MAR regional atmospheric model outputs and to MODIS albedo retrievals.  
19 Using different albedo parameterizations, we performed offline ES simulations forced by the MAR model over  
20 the 2000-2019 period. Our results reveal a strong sensitivity of the modeled SMB components to the albedo  
21 parameterization. Results inferred with albedo parameters obtained with a manual tuning approach present a very  
22 good agreement with the MAR outputs. Conversely, with the albedo parameterization used in the standard  
23 ORCHIDEE version, runoff and sublimation were underestimated. We also tested parameters found from a  
24 previous data assimilation experiment calibrating the ablation processes using MODIS snow albedo. While these  
25 parameters greatly improve the modelled albedo over the entire ice sheet, they degrade the other model outputs  
26 compared to those obtained with the manually-tuned approach. This is likely due to the model overfitting to the  
27 calibration albedo dataset without any constraint applied to the other processes controlling the state of the  
28 snowpack. This underlines the need for performing a “multi-objective” optimisation using auxiliary observations  
29 related to snowpack internal processes. Although there is still room for further improvements, the developments  
30 reported in the present study constitute an important advance in assessing the Greenland SMB with possible  
31 extension to mountain glaciers or the Antarctic ice sheet.

## 32 1. Introduction

33 Satellite observations reveal that the Greenland ice sheet (GrIS) has been losing mass for at least three decades.  
34 Between 1992 and 2018, the net ice mass loss was estimated at  $3800 \pm 339$  Gt, corresponding to a rise in global  
35 mean sea level of  $10.6 \pm 0.9$  mm (The IMBIE team, 2020). Mass loss is driven by dynamic solid ice discharges  
36 (Enderlin et al., 2014) and by enhanced surface meltwater and runoff (Ryan et al., 2019). Over the 2000-2008  
37 period, the GrIS mass loss was equally partitioned between surface and dynamic processes (van den Broeke et al.,



38 2009). However, recent studies based on regional climate models and remote sensing observations (van den  
39 Broeke, 2016; Ryan et al., 2019; The IMBIE Team, 2020, Fox-Kemper et al., 2021) show that rates of mass change  
40 are now dominated by changes in surface mass balance (SMB), defined as the difference between mass gains (solid  
41 and liquid precipitation) and surface ablation processes (runoff, sublimation and snow erosion).

42 Besides directly impacting the global mean sea level, the GrIS is also an integral part of the Earth System (Fyke  
43 et al., 2018). As such, it is highly sensitive to climate change and in turn, has a strong influence on global climate,  
44 notably by releasing fresh water into the ocean, which leads to changes in the Atlantic meridional overturning  
45 circulation (Bakker et al., 2016; Martin et al., 2022). Surface melting may also induce changes in the local climate  
46 through the temperature-elevation feedback (Edwards et al., 2014; Sellevod et al., 2019) and the albedo effect  
47 (Box et al., 2012; Helsen et al., 2017; Riihelä et al., 2019). Finally, changes in topography produce modifications  
48 of the local and large-scale atmospheric circulations (Ridley et al., 2005; Hahn et al., 2020).

49 To capture these feedbacks and to reduce the uncertainties in sea-level and climate projections, a key objective of  
50 the climate-ice sheet modelling community is to incorporate ice-sheet models in Earth System Models (ESMs)  
51 (Vizcaino, 2014). Such coupled climate-ice sheet models have mainly been developed with low resolution climate  
52 models designed for long-term integrations (Kageyama et al., 2004; Charbit et al., 2005; Vizcaino et al., 2010;  
53 Roche et al., 2014). So far, only a few groups have met this goal with CMIP-like models (Vizcaino et al., 2013;  
54 Muntjewerf et al., 2020; Smith et al., 2021). A key challenge in developing such models relates to the realistic  
55 computation of SMB used as a forcing field of the ice-sheet models.

56 SMB is highly dependent on the radiative properties of snow and on the physical processes occurring within the  
57 snowpack (Helsen et al., 2017). At the surface, snow cover evolves as a function of the surface energy balance and  
58 mass exchanges with the atmosphere. In cold regions, snow melt is largely driven by shortwave radiation: Because  
59 of the high albedo value of fresh snow (0.80 – 0.90), a large fraction of shortwave radiation is reflected to the  
60 atmosphere, limiting the energy available at the surface for melting. Therefore, snow evolution is strongly  
61 dependent on the albedo. The value of snow albedo decreases when snow is ageing (i.e., in the absence of a new  
62 snowfall event), and with the snow metamorphism and liquid water content at the ice sheet's surface coming either  
63 from rainfall or from snow/ice melting. Surface water may also percolate and refreeze inside the snowpack, thereby  
64 delaying the runoff. The transformation of snow into ice depends on environmental conditions (e.g., winds, near-  
65 surface temperatures) and internal processes within the snowpack (e.g., heat conduction and vertical temperature  
66 gradient, compaction), which directly influence the grain microstructure and the snow density. All these processes  
67 affect the SMB of the ice sheet.

68 There are several ways to compute the SMB. Empirical approaches such as the positive degree-day method (Reeh,  
69 1991) have long been used to compute snow and ice melting from downscaled near-surface temperatures. This  
70 kind of approach requires little computational resources and has often been applied for past and future long-term  
71 integrations (Charbit et al., 2008; 2013; Bonelli et al., 2009; Vizcaino et al., 2010). However, such methods have  
72 been calibrated against the present state of the GrIS, raising the question as to whether they can be applied in a  
73 different climatic context from the present-day one knowing that ablation is projected to increase (van de Wal,  
74 1996; Bougamont et al., 2007). Moreover, they are not physically-based and cannot reproduce the diversity of  
75 snow processes that directly influence the SMB. Snow models implemented in general circulation models have  
76 long been based on simplified physics. They are mainly designed to resolve the seasonal and diurnal variations of  
77 heat fluxes, but with no representation of internal processes (Armstrong and Brun, 2008). By contrast, regional



78 climate models developed for polar regions generally incorporate multiple-layer energy balance snow models with  
79 a fine vertical resolution (e.g., Brun et al., 1992; Lefebre et al., 2003; Vionnet et al., 2012; Noël et al., 2018) and  
80 with detailed snow physics to simulate a variety of snowpack processes. However, due to their high computational  
81 cost, they are not used in ESMs, despite a few rare attempts (Punge et al., 2012). An alternative approach consists  
82 in implementing snow models of intermediate complexity in the land surface components of ESMs (Boone and  
83 Etchevers, 2001; Dutra et al., 2010; Wang et al., 2013; Cullather et al., 2014; Decharme et al., 2016; Born et al.,  
84 2019). These models have a limited number of layers and are based on simplified representations of the main  
85 processes affecting the SMB changes, but usually do not have any explicit representation of snow metamorphism.  
86 However, they offer a good compromise between models of high complexity and simplified approaches or bulk-  
87 layer models for coupling with atmospheric models.

88 The snow module Explicit Snow (referred hereafter to as ES) implemented in the land surface model ORCHIDEE  
89 (Organising Carbon and Hydrology In Dynamic Ecosystems; Krinner et al., 2005; Chéruy et al., 2020) of the  
90 IPSL-CM ESM (Boucher et al., 2020) belongs to this third class of snow models. It has been successfully evaluated  
91 against observations in Col de Porte (French Alps) and in various sites of Northern Eurasia (Wang et al., 2013).  
92 However, it has not yet been adapted to ice-covered areas. As a result, glaciers are considered as bare soils in the  
93 current ORCHIDEE version, and over ice sheets, snow is handled with the atmospheric component of IPSL-CM  
94 in a very simplistic way. Recently, we made new developments to apply the ES model to glaciers and ice sheets,  
95 with a special focus on the GrIS. These developments meet two objectives. The first one is to treat snow-related  
96 processes in IPSL-CM in a more consistent way for all surface types. The second one is to compute the SMB,  
97 taking the main processes occurring within the snowpack into account. These developments also constitute a  
98 preliminary step for the subsequent use of the computed SMB as an interface between IPSL-CM and ice-sheet  
99 models. In the following, we will refer to ORCHIDEE-ICE to deal with the version of ORCHIDEE that includes  
100 these new developments, and to ORCHIDEE to deal with the former version of the model.

101 In this study, we evaluate the computation of SMB (and its components) in the ES model. As SMB is strongly  
102 dependent on the albedo, we also examine its sensitivity to various albedo parameterizations. To achieve this, we  
103 performed offline ORCHIDEE-ICE simulations and compared our results against model outputs from the polar-  
104 oriented regional atmospheric model MARv3.11.4 (Modèle Atmosphérique Régional, Fettweis et al., 2017) and  
105 the MODIS (MODerate resolution Imaging Spectroradiometer, Hall et al., 1995; Hall and Riggs, 2016) surface  
106 albedo retrievals. The paper is organized as follows. In Section 2, we provide an extensive description of the main  
107 characteristics of the original ES model as well as changes that occurred since its early publication (Wang et al.,  
108 2013). The new developments made for applying ES to the GrIS are also presented in this section. Section 3  
109 describes the experimental setup and Section 4 provides a brief overview of the different datasets used for  
110 evaluation. The results are presented in Sections 5 and 6 and discussed in Section 7.

## 111 2. Model description

### 112 2.1 Snow processes in the current ORCHIDEE-AR6 model

113 ORCHIDEE is the land surface component of IPSL-CM Earth System Model (Boucher et al., 2020; Chéruy et al.,  
114 2020) mainly developed at the French Institute Pierre Simon Laplace (IPSL). It computes both the water and  
115 energy exchanges (SECHIBA module) between land surfaces and the atmosphere at a half-hourly time step and



116 includes carbon-related processes (STOMATE module). Within a given grid cell, land cover is represented as  
117 fractions of bare soils and vegetated areas described in terms of plant functional types (PFTs). The snow-vegetation  
118 interactions are not explicitly represented and snow is evenly distributed among the various PFTs. Soil types are  
119 prescribed according to the USDA soil texture maps (Reynolds et al., 2000). The ORCHIDEE model can be run  
120 in off-line mode, driven by atmospheric fields, or coupled with an atmospheric model. In the former ORCHIDEE  
121 version used for CMIP5 (Taylor et al., 2012), the snow scheme over glaciated surfaces was based on the bulk  
122 approach proposed by Chalita and Le Treut (1994). It consisted of a composite soil-snow model accounting for  
123 the thermal and radiative properties of snow cover (i.e., albedo and its variations with snow ageing). Snow was  
124 described as having a constant density ( $330 \text{ kg m}^{-3}$ ) and melting occurred when temperature exceeded  $0^\circ\text{C}$ . Other  
125 processes such as water percolation and refreezing were ignored, although they directly impact the water budget.  
126 This means that all liquid water coming from melting snow was leaving the snowpack as runoff.

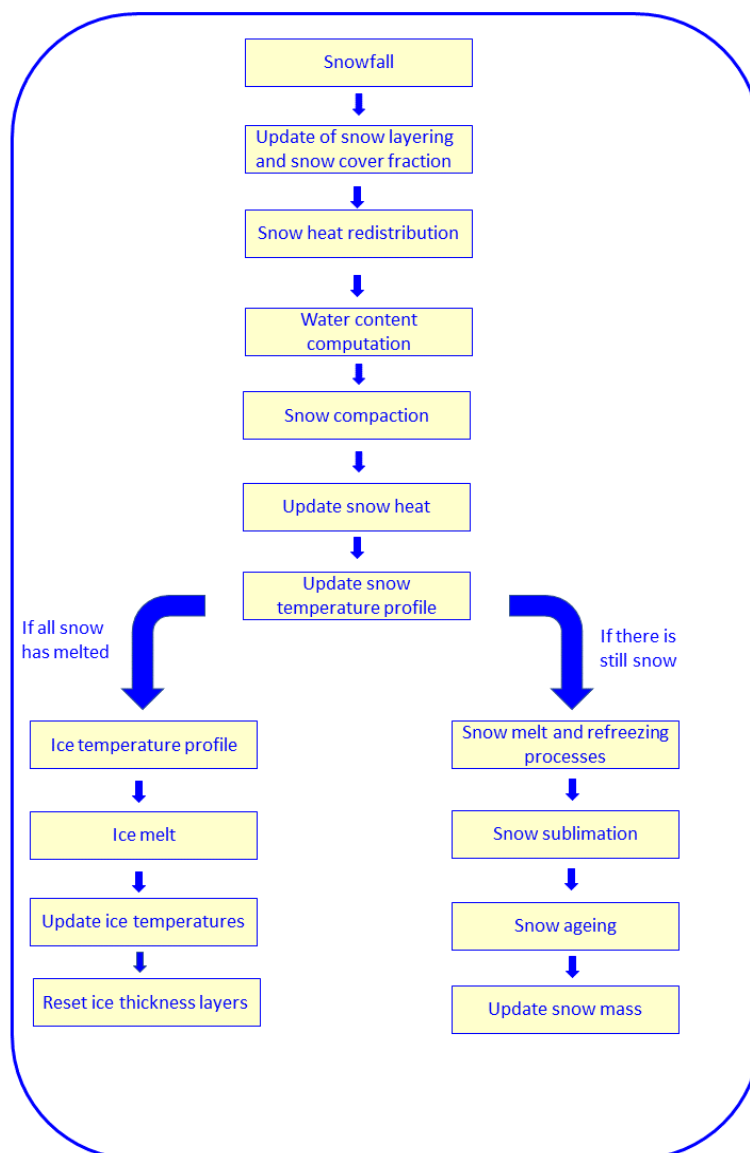
127 For the CMIP6 exercise (Eyring et al., 2016), the bulk approach has been replaced by the ES snow scheme, which  
128 was formerly adapted to the ORCHIDEE architecture (Wang et al., 2013) from a three-layer version of the ISBA-  
129 ES scheme (Interactions between Soil, Biosphere and Atmosphere-Explicit Snow scheme; Boone and Etchevers,  
130 2001) developed at the French National Center for meteorological Research. The ES model is now used in the  
131 standard version of ORCHIDEE (version 2.0 onwards). However, it has not yet been considered for use over  
132 mountainous glaciers, which are treated as bare soils, nor over ice sheet areas, which are currently handled by the  
133 LMDZ atmospheric model (Ch eruy et al., 2020) with a very elementary snow scheme (i.e., single-layer model,  
134 constant albedo and thermal conductivity). In this section, we provide an extensive description of the snow model,  
135 including the main differences with the original ISBA-ES version (Wang et al., 2013). The new developments  
136 accounting for snow processes over ice-covered areas in the ORCHIDEE model are described in section 2.2.

137 The ES model represents the snowpack as a one-dimensional physical system (vertical coordinate  $z$ ). This means  
138 that all the lateral fluxes of mass and energy are ignored. The original version of this snowpack is discretized in  
139 three layers following the parameterization of Lynch-Stieglitz (1994), which sets the upper limits for the thickness  
140 of the first two layers at 5 and 50 cm respectively. This ensures the propagation of variations in the diurnal cycle  
141 of temperature and radiation, and enables vertical heat and density gradients, which are assumed to be larger near  
142 the surface, to be resolved correctly. Each layer is described in terms of snow density, snow age, layer thickness,  
143 heat content, snow temperature and liquid water content, with the first three variables being prognostic variables.  
144 Changes in snow mass are determined by the snowfall rate, snow melting, runoff at the base of the snowpack and  
145 sublimation at the surface. In the absence of coupling with a dynamic ice sheet model, snow mass at the surface  
146 of the ice sheet can be overestimated. Thus, to prevent excessive snow accumulation, we impose a maximum  
147 threshold of  $3000 \text{ kg m}^{-2}$  beyond which snow is artificially removed. An overview of the organization of the  
148 different subroutines of the ES snowpack model is provided in Figure 1. The description of the processes is given  
149 in the following subsections and the list of model parameters is provided in Table A1 (Appendix A).

150



## Explicit Snow



151

152 **Figure 1:** Flowchart of the new Explicit Snow scheme implemented in the ORCHIDEE-ICE model.

153

154

155

156



## 157 2.1.1 Surface processes

### 158 **Energy balance**

159 The evolution of the snowpack is primarily driven by the energy flux at the snow-atmosphere interface. A single  
160 energy balance is computed for all surface types coexisting in one grid cell. The surface energy flux ( $G_{surf}$ )  
161 available at the snow-atmosphere interface is computed from the energy balance equation:

$$162 \quad G_{surf} = SW_{net} + LW_{net} - H_L - H_S + H_{rainfall} \quad (1)$$

163  $G_{surf}$  is computed negatively when it cools the atmosphere (i.e., warms the surface).  $SW_{net}$  and  $LW_{net}$  are the net  
164 shortwave and longwave radiations respectively,  $H_L$  is the latent heat flux,  $H_S$  is the sensible heat flux and  $H_{rainfall}$   
165 is the energy released by rainfall (see Eq. (14) in Boone and Etchevers, 2001). Equation (1) is used to compute the  
166 surface temperature ( $T_{surf}$ ) of the grid cell at the next time step and provides the limit condition of the surface  
167 temperature at the snow-atmosphere interface for the calculation of the snow temperature profile.

168 Above snow-covered surfaces, when  $T_{surf}$  is above the freezing temperature  $T_0$  (273.15 K), the energy excess is  
169 first used to bring the snow temperature to  $T_0$ . A surface energy flux  $G_{freezing}$  associated with the freezing  
170 temperature  $T_0$  can be computed using a similar formulation to Eq. (1). The difference between  $G_{surf}$  and  $G_{freezing}$   
171 is converted in an additional temperature expressed as:

$$172 \quad T_{snow}^{add} = T_{surf} - T_0 = \frac{G_{surf} - G_{freezing}}{C_{soil}} dt \quad (2)$$

173  $C_{soil}$  is the surface heat capacity of soil ( $J m^{-2} K^{-1}$ ) and is computed as the sum of heat capacities for snow-covered  
174 and snow-free surfaces (for both non-glaciated and glaciated areas) weighted by their respective grid cell fractions.  
175 For snow-covered surfaces, the specific heat capacity is defined as the product of snow density and the specific  
176 heat of ice ( $2106 J K^{-1} kg^{-1}$ ). If  $T_{snow}^{add}$  is greater than (or equal to) the freezing temperature, the energy excess is  
177 used for melting snow, and  $G_{surf}$  is further set to  $G_{freezing}$  for energy conservation. If the new  $G_{surf}$  value is  
178 greater than the total heat content of the snowpack, snow is entirely melted and the excess energy is transferred to  
179 the underlying soil. The energy released by snowfall is accounted for in the snowpack scheme to update the snow  
180 heat content of the snowpack after a snowfall event.

### 181 **Turbulent heat fluxes**

182 The sensible ( $H_S$ ) and latent heat ( $H_L$ ) fluxes computed for each grid cell are given respectively by:

$$183 \quad H_S = \rho_{air} q_{cdrag} U (T_{surf} - T_{air}) \quad (3)$$

$$184 \quad H_L = L_s \rho_{air} q_{cdrag} U (Q_{sat} - Q_{air}) \quad (4)$$

185 where  $\rho_{air}$  is the air density,  $T_{surf}$  and  $T_{atm}$  are the surface and the 2 m atmospheric temperatures,  $Q_{air}$  and  $Q_{sat}$   
186 are the air specific humidity at 2 m and the saturated specific humidity at the surface,  $L_s$  is the latent heat of  
187 sublimation ( $2.8345 \cdot 10^6 J kg^{-1}$ ),  $U$  is the wind speed at 10 m and  $q_{cdrag}$  is the drag coefficient computed as a  
188 function of the ice roughness length ( $z0_{ice} = 0.001 m$ ), following the Monin-Obukhov turbulence theory (Monin  
189 and Obukhov, 1954) and the parameterizations of the eddy fluxes proposed by Louis (1979).

### 190 **Snow sublimation**

191 The amount of sublimation is simply deduced from the latent heat flux:



$$192 \quad S_{snow} = \frac{H_L}{L_s} \quad (5)$$

193 **Snow cover fraction**

194 The snow cover fraction ( $F_{snow}$ ) is derived from the formulation of Niu and Yang (2007) which has been shown  
 195 to better represent the seasonal variation of the relationship between snow depth ( $Z_{snow}$ ) and snow cover fraction  
 196 thanks to its dependence on snow density:

$$197 \quad F_{snow} = \tanh\left(\frac{Z_{snow}}{2.5z_{og} \times \left(\frac{\rho_{snow}}{\rho_{min}}\right)^m}\right) \quad (6)$$

198 where  $\rho_{snow}$  is the snow density averaged over the total thickness of the snowpack,  $\rho_{min}$  is the minimum snow  
 199 density (set to  $50 \text{ kg m}^{-3}$ ), that is the density of fresh snow,  $z_{og}$  is the ground roughness length (set to 0.01 m) and  
 200  $m$  (set to 1.0 in the present study) is an adjustable parameter.

201 **Snow albedo**

202 Compared to the early version presented in Wang et al. (2013), the albedo scheme has been modified and snow  
 203 albedo is now computed following the formulation of Chalita and Le Treut (1994):

$$204 \quad \alpha_{snow} = A_{aged} + B_{dec} \exp\left(-\frac{\tau_{snow}}{\tau_{dec}}\right) \quad (7)$$

205 where  $A_{aged}$  represents the albedo of a snow-covered surface after snow ageing (old snow) and  $B_{dec}$  is defined so  
 206 that the sum of  $A_{aged}$  and  $B_{dec}$  represents the albedo of fresh snow (i.e., maximum snow albedo).  $\tau_{dec}$  is the time  
 207 constant of the albedo decay and  $\tau_{snow}$  is the snow age and is parameterized as follows:

$$208 \quad \tau_{snow}(t + dt) = \left[\tau_{snow}(t) + \left(1 - \frac{\tau_{snow}}{\tau_{max}}\right) \times dt\right] \times \exp\left(-\frac{P_{snow}}{\delta_c}\right) + f_{age} \quad (8)$$

209 where  $\tau_{max}$  is the maximum snow age,  $P_{snow}$  is the amount of snowfall during the time interval  $dt$  and  $\delta_c$  is the  
 210 critical value of solid precipitation necessary for resetting the snow age to zero (i.e., no ageing for fresh snow). In  
 211 addition, low surface air temperatures found in polar regions slow down the metamorphism. This effect is  
 212 accounted for with the function  $f_{age}$  expressed as:

$$213 \quad f_{age} = \left[\frac{(\tau_{snow}(t) + (1 - \frac{\tau_{snow}}{\tau_{max}}) \times dt) \times \exp(-\frac{P_{snow}}{\delta_c}) - \tau_{snow}(t)}{1 + g_{temp}(T_{surf})}\right] \quad (9)$$

$$214 \quad g_{temp}(T_{surf}) = \left[\frac{\max(T_0 - T_{surf}, 0)}{\omega_1}\right]^{\omega_2} \quad (10)$$

215 where  $\omega_1$  and  $\omega_2$  are tuning constants. The albedo is computed for the visible and near-infrared spectral bands.  
 216 However, to compute the upward shortwave radiation, an arithmetic mean between the visible and the near-  
 217 infrared albedo is considered.

218 A single energy balance is computed for all surface types but the albedo is weighted by the different fractions of  
 219 PFTs and glaciated areas and by the snow-covered and snow-free fractions. As a result, the surface albedo ( $\alpha$ ) of  
 220 the grid cell is computed as the sum of snow-free albedo ( $\alpha_{snow-free}$ ) and snow-covered albedo ( $\alpha_{snow}$ ) weighted  
 221 by the fractional area of the grid cell covered by snow  $F_{snow}$  (snow-covered fraction hereafter):



$$222 \quad \alpha = F_{snow} \times \alpha_{snow} + (1 - F_{snow}) \times \alpha_{snow-free} \quad (11)$$

223 with:

$$224 \quad \alpha_{snow} = f_{ice} \times \alpha_{snow}^{ice} + \sum_{PFT} f_{PFT,i} \times \alpha_{snow}^{PFT,i} \quad (11a)$$

225 and:

$$226 \quad \alpha_{snow-free} = f_{ice} \times \alpha_{snow-free}^{ice} + \sum_{PFT} f_{PFT,i} \times \alpha_{snow-free}^{PFT,i} \quad (11b)$$

227  $f_{ice}$  and  $f_{PFT,i}$  are the grid cell fractions of ice-covered areas and the  $i^{th}$  PFT respectively;  $\alpha_{snow}^{ice}$  (resp.  $\alpha_{snow-free}^{ice}$ )

228 and  $\alpha_{snow}^{PFT,i}$  (resp.  $\alpha_{snow-free}^{PFT,i}$ ) are the corresponding snow albedo (resp. snow-free albedo) values.

229 Over the GrIS,  $\alpha_{snow-free}$  is given by the albedo of bare ice, prescribed to 0.6 and 0.2 for visible and near-infrared  
 230 wavelengths respectively. At the margins of the GrIS, some grid points may be only partially covered by snow or  
 231 ice, or even become totally snow-free during the melting season. It is therefore important to take these different  
 232 features into account to compute correctly the surface albedo of the GrIS.

### 233 2.1.2 Internal processes

234 When snow falls on a snow-free surface, a new snowpack is generated providing that the ground temperature is  
 235 below or equal to the freezing point. The snow mass and the heat content of the snowfall are initially distributed  
 236 evenly within the three layers. The snow density is the same for the three layers and is given by the density of the  
 237 snowfall computed as a function of wind speed and surface air temperature (Pahaut, 1976). When snowfall occurs  
 238 over an existing snowpack, fresh snow is added to the upper layer and the snow age is reset to zero providing that  
 239 the snowfall thickness is greater than the critical threshold  $\delta_c$  (see Eq. 8). The snow thickness, density and heat  
 240 content are then modified in this layer. However, as the number of snow layers is kept fixed, redistribution of mass  
 241 and heat content within the layers is required when snow depth changes, but the total snow mass and heat content  
 242 are conserved.

#### 243 Heat conduction

244 The heat conduction from the surface to the bottom of the snowpack is described by a vertical diffusion equation  
 245 relating the temporal evolution of the snow temperature in the snowpack at a depth  $z$  and the divergence of the  
 246 snow heat flux  $F_C$  and is solved using an implicit numerical scheme.

$$247 \quad \frac{\partial T_{snow}}{\partial t} = - \frac{1}{C_{snow}} \cdot \frac{\partial F_C}{\partial z} \quad (12)$$

$$248 \quad F_C = - \Lambda_s \frac{\partial T_{snow}}{\partial z} \quad (13)$$

249 with  $C_{snow}$  ( $J m^{-2} K^{-1}$ )  $\Lambda_s$  and  $T_{snow}$  being the snow heat capacity, the snow thermal conductivity ( $W m^{-1} K^{-1}$ ) and  
 250 the snow temperature respectively.

251 At the snow-atmosphere interface, the boundary condition is given by the energy balance equation ( $F_C = G_{surf}$ )  
 252 and is used in the ORCHIDEE model to compute the surface temperature.

253 Along with the thermal gradient, a water vapor diffusive flux takes place from the warmer to the colder parts of  
 254 the snowpack and sublimation or condensation may occur in the pore spaces depending on the water vapor  
 255 saturation pressure. This process is particularly significant in the Arctic because of strong temperature gradients





256 between soils and atmosphere and is in great part responsible for snow metamorphism. While it is explicitly  
 257 accounted for in detailed snow models, in Explicit Snow, the effect of water vapor diffusion and phase changes is  
 258 parameterized through the thermal conductivity (Sun et al., 1999). An effective thermal conductivity ( $\Lambda_{eff}$ ) is thus  
 259 expressed as the sum of empirical formulations for snow thermal conductivity ( $\Lambda_{cond}$ ) and thermal conductivity  
 260 from vapor transport ( $\Lambda_{vap}$ ), with:

$$261 \quad \Lambda_{cond}^i = a_\lambda + b_\lambda \rho_{snow}^i{}^2 \quad (14)$$

$$262 \quad \Lambda_{vap}^i = \left( a_{\lambda v} + \frac{b_{\lambda v}}{c_{\lambda v} + T_{snow}^i} \right) \frac{P_0}{P} \quad (15)$$

263 With  $a_\lambda = 0.02 \text{ W m}^{-1} \text{ K}^{-1}$ ,  $b_\lambda = 2.5 \cdot 10^{-6} \text{ W m}^5 \text{ K}^{-1} \text{ kg}^{-2}$  (Anderson, 1976),  $a_{\lambda v} = -0.06023 \text{ W m}^{-1} \text{ K}^{-1}$ ,  $b_{\lambda v} = -2.5425$   
 264  $\text{W m}^{-1}$  and  $c_{\lambda v} = -289.99 \text{ K}$  (Yen, 1981).  $P$  is the atmospheric pressure in hPa and  $P_0 = 1000 \text{ hPa}$ . The superscripts  
 265  $i$  denote the  $i^{th}$  layer.

#### 266 **Heat content**

267 The heat content is computed using the following equation:

$$268 \quad H_{snow}^i = D_{snow}^i [C_{snow}^{v,i} (T_{snow}^i - T_f) - L_s \rho_{snow}^i] + L_f \rho_{water} W_{liq}^i \quad (16)$$

269 where  $L_f$  is the latent heat of fusion and  $\rho_{water}$  is the water density.  $H_{snow}^i$ ,  $W_{liq}^i$ ,  $D_{snow}^i$ ,  $\rho_{snow}^i$  and  $C_{snow}^{v,i}$  are  
 270 the heat and liquid contents, the depth, the density and the mean volumetric heat capacity ( $\text{J K}^{-1} \text{ m}^{-3}$ ) of the  $i^{th}$   
 271 layer.

272 After heat redistribution within the snowpack, snow temperature is diagnosed using Eq. (16), assuming no liquid  
 273 water in the snowpack. If snow temperature exceeds the freezing point, the liquid content in each layer is then  
 274 diagnosed from the snow temperature and heat content of the layer, and the temperature is then reset to the freezing  
 275 point.

#### 276 **Compaction**

277 The total snow depth decreases as density increases. Changes in density occur as a result of the weight of the  
 278 overlying snow layers and under the influence of snow metamorphism. The local rate of density change in the  $i^{th}$   
 279 layer is derived from Anderson (1976):

$$280 \quad \frac{1}{\rho_{snow}^i} \frac{\partial \rho_{snow}^i}{\partial t} = \frac{\sigma_{snow}^i}{\eta_{snow}^i (T_{snow}^i, \rho_{snow}^i)} + \psi_{snow}^i (T_{snow}^i, \rho_{snow}^i) \quad (17)$$

281 The first term of the right-hand side represents the compaction due to snow load, with  $\sigma_{snow}^i$  (Pa) being the pressure  
 282 of the overlying snow and  $\eta_{snow}^i$  the snow viscosity.

$$283 \quad \sigma_{snow}^i = g \times M_{snow}^i$$

284 where  $g$  is the gravitational constant ( $\text{m s}^{-2}$ ) and  $M_{snow}^i$  the cumulative snow mass ( $\text{kg m}^{-2}$ ).

285 The viscosity (in Pa s) is expressed as a function of snow temperature and density (Mellor, 1964; Kojima, 1967):

$$286 \quad \eta_{snow}^i = \eta_0 \exp[a_\eta (T_f - T_{snow}^i) + b_\eta \rho_{snow}^i] \quad (18)$$

287 with  $\eta_0 = 3.7 \times 10^7 \text{ Pa s}$ ,  $a_\eta = 8.1 \times 10^{-2} \text{ K}^{-1}$  and  $b_\eta = 1.8 \times 10^{-2} \text{ m}^3 \text{ kg}^{-1}$ .



288 The second term in the right-hand side of Eq. (17) parameterizes the effect of metamorphism which is significant  
 289 for newly fallen snow.

$$290 \quad \psi_{snow}^i = a_\psi \exp[-b_\psi \cdot (T_f - T_{snow}^i) - c_\psi \cdot \max(0, \rho_{snow}^i - \rho_\psi)] \quad (19)$$

291 The values of the parameters are the following:  $a_\psi = 2.8 \times 10^{-6} \text{ s}^{-1}$ ,  $b_\psi = 4.2 \times 10^{-2} \text{ K}^{-1}$ ,  $c_\psi = 460 \text{ m}^3 \text{ kg}^{-1}$ ,  $\rho_\psi = 150$   
 292  $\text{kg m}^{-3}$ .

293 In the model, density changes due to compaction are allowed as long as density remains below a threshold fixed  
 294 to  $750 \text{ kg m}^{-3}$ . Compaction does not affect the total mass and the heat content of the snowpack but changes the  
 295 layer thicknesses. The distribution of snow heat within the layers must therefore be updated using Eq. (16).

### 296 *Vertical temperature profile*

297 The snow temperature profile resulting from heat redistribution is then computed by solving the heat diffusion  
 298 equation using an implicit numerical scheme similar to that used for heat diffusion in the soil. The vertical  
 299 temperature profile within the snowpack is expressed as:

300 For the 1<sup>st</sup> layer:

$$301 \quad T_{snow}^1 = \left[ \frac{\lambda_{snow} \cdot C_{gr\_snow} + (T_{surf} + T_{snow}^{add})}{1 + \lambda_{snow} (1 - D_{gr\_snow})} \right] \quad (20)$$

302 For the deeper layers ( $i > 1$ ):

$$303 \quad T_{snow}^{i+1} = C_{gr\_snow} + D_{gr\_snow} \cdot T_{snow}^i \quad (21)$$

304 where  $\lambda_{snow}$ ,  $C_{gr\_snow}$ ,  $D_{gr\_snow}$  are coefficients resulting from the resolution of the numerical scheme and depend  
 305 on the snow heat capacity and thermal conductivity and on the characteristics of the vertical discretization.

### 306 *Melt and refreezing processes*

307 If melt water is produced at the surface, it may remain in the liquid state in the uppermost layer or penetrate in the  
 308 next layer where it can remain or refreeze as long as the maximum water holding capacity is not reached; otherwise  
 309 it penetrates in the lower layers.

310 The evolution of liquid water in each layer is controlled by the energy required to induce phase changes and by  
 311 the maximum water holding capacity. In the  $i^{\text{th}}$  layer, the energy used for melting snow ( $E_{snow}^i$ ) is expressed as:

$$312 \quad E_{snow}^i = \min \left( C_{snow}^{v,i} D_{snow}^i \times \max(0, T_{snow}^i - T_f), \max(0, D_{swe}^i - W_{liq}^i) \times L_f \rho_{water} \right) \quad (22)$$

313 where  $D_{swe}^i$  is the snow water equivalent in the  $i^{\text{th}}$  layer. The first term represents the available energy for phase  
 314 change in the  $i^{\text{th}}$  layer and the second term corresponds to the energy required to melt entirely the snow mass that  
 315 has not been transformed into liquid water. The maximum water holding capacity is taken from Anderson (1976):

$$316 \quad W_{max}^i = \left[ r_{min} + (r_{max} - r_{min}) \cdot \max \left( 0, \frac{\rho_t - \rho_{snow}^i}{\rho_t} \right) \right] \cdot \frac{\rho_{snow}^i}{\rho_w} \cdot D_{snow}^i \quad (23)$$

317 with  $r_{min} = 0.03$ ,  $r_{max} = 0.10$  and  $\rho_t = 200 \text{ kg m}^{-3}$ .

318 Runoff ( $S_{melt}$ ) is computed as the sum of meltwater produced at the surface and the total liquid water that has  
 319 percolated down to the bottom layer and that exceeds  $W_{max}^{bottom}$ . It is thus simply given by:

$$320 \quad S_{melt} = \frac{\sum_i E_{snow}^i}{L_f} \quad (24)$$



321 At each time step, changes in layer thickness, density and liquid water content in each layer are updated as well as  
 322 changes in snow temperature due to melting or refreezing. In case of complete snow melting, the energy excess  
 323 that has not been used for phase changes is used to warm the underlying ground.

## 324 2.2 New developments

### 325 2.2.1 New snow layering scheme

326 As mentioned in Section 1, snow models of intermediate complexity are a good compromise between detailed  
 327 snow models and single-layer models. They are designed to be implemented in ESMs and, as such, should not  
 328 require excessive computational time. Although their vertical resolution is generally limited to five layers at most  
 329 (Cristea et al., 2022), several studies reported that snow models of intermediate complexity considerably improve  
 330 the representation of basic features of the snowpack and reduce biases in surface temperature when they are  
 331 compared to single-layer models (Lynch-Stieglitz, 1994; Boone and Etchevers, 2001; Dutra et al., 2012; Wang et  
 332 al., 2013). Despite these good performances, increasing the number of snow layers (with finer layers near the  
 333 surface or near the snow/ice interface) is expected to improve the modeled heat conduction within the snowpack,  
 334 the simulated temperature at the snow/ice interface, and subsequently the vertical temperature profile in the ice  
 335 and eventually the simulated SMB (Cristea et al., 2022). We therefore increased the number of snow layers from  
 336 3 to 12, following the layering scheme proposed by Decharme et al. (2016) for ISBA-ES in which the new layering  
 337 scheme is defined as:

$$338 \left\{ \begin{array}{l} D_{snow}^i = \min\left(\delta_i, \frac{Z_{snow}}{12}\right) \text{ for } i \leq 5 \text{ or } i \geq 9 \\ D_{snow}^6 = 0.3d_r - \min(0, 0.3d_r - D_{snow}^5) \\ D_{snow}^7 = 0.4d_r + \min(0, 0.3d_r - D_{snow}^5) - \min(0, 0.3d_r - D_{snow}^9) \\ D_{snow}^8 = 0.3d_r - \min(0, 0.3d_r - D_{snow}^9) \\ d_r = Z_{snow} - \sum_{i=1}^5 D_{snow}^i - \sum_{i=9}^{12} D_{snow}^i \end{array} \right. \quad (25)$$

339 The  $\delta_i$  values correspond to the maximum widths of the layers 1 to 5 and 9 to 12 and are fixed to  $\delta_1 = 0.01$  m,  
 340  $\delta_2 = 0.05$  m,  $\delta_3 = 0.15$  m,  $\delta_4 = \delta_{10} = 0.5$  m,  $\delta_5 = \delta_9 = 1$  m,  $\delta_{11} = 0.1$  m, and  $\delta_{12} = 0.02$  m. For very thin  
 341 snowpacks ( $Z_{snow} \leq Z_{thin} = 0.1$  m), each layer has the same thickness  $\frac{Z_{thin}}{12}$ . The layer thickness are updated at  
 342 each time step if the first two layers ( $i = 1, 2$ ) or the bottom layer ( $i = 12$ ) become too thin  
 343 (*less than*  $D_{snow}^i = 0.5 \times \left(\delta_i, \frac{Z_{snow}}{12}\right)$ ) or too thick (*larger than*  $D_{snow}^i = 1.5 \times \left(\delta_i, \frac{Z_{snow}}{12}\right)$ ). In that case, the  
 344 snow mass and heat content are redistributed according to the new layering scheme. Otherwise, the layer  
 345 thicknesses at the current time step are kept to their previous values (i.e., at the previous time step). This allows to  
 346 maintain the density and thermal conductivity of fresh snow as long as the depth has not changed too much. This  
 347 enables the model to work more closely with more complex models in which new snow layers are associated with  
 348 a new snowfall event.

349

350



### 351 2.2.2 Implementation of ice layers

352 In case the snow mass has completely melted, ice melting occurs if the available energy is sufficient and contributes  
353 to runoff. To account for the presence of ice below the snow layers, we implemented a new module in ORCHIDEE  
354 to compute the heat diffusion and the vertical temperature distribution in the ice as well as the potential ice melting.  
355 This module works in a similar way as the ES model and only accounts for vertical fluxes. The ice reservoir is  
356 discretized into eight layers whose maximum thicknesses are fixed to 0.01, 0.05, 0.15, 0.5, 1, 5, 10 and 50 m. A  
357 finer vertical spacing is imposed for the upper layers to better resolve heat conduction at the snow-ice or  
358 atmosphere-ice interface. The large thickness of the bottom layer allows it to have an almost constant temperature  
359 throughout the year as it has been observed at a few tens of meters depth (Patterson, 1994). Ice layers are only  
360 implemented above an icy soil-type. If the icy soil is predominant in a given grid cell, then the entire surface  
361 corresponding to this grid point will be considered as icy.

362 In the absence of a dynamic ice model that transports ice from the interior of the ice sheet (or glacier) to the edges,  
363 the total ice mass may disappear entirely in the ablation zones especially in long-term simulations. To avoid such  
364 situations, ice is considered as an infinite reservoir: melting ice contributes to runoff but, at each time step, the  
365 amount of ice melted in the upper layers is counterbalanced by ice added at the base, and the layer thicknesses are  
366 kept fixed to their initial value.

367 The vertical distribution of temperature is determined using the same numerical scheme as that for the snowpack.  
368 If snow is still present over the ice soil, the temperature in the top ice layer is given by the temperature of the  
369 bottom snow layer computed using Eq. (21). If snow has completely melted, the temperature in the first ice layer  
370 is given by an expression similar to Eq. (20):

$$371 T_{ice}^1 = \left[ \frac{\lambda_{ice} C_{gr\_ice} (T_{surf} + T_{snow}^{add})}{1 + \lambda_{ice} (1 - D_{gr\_ice})} \right] \quad (26)$$

372 For the deeper layers, the ice temperature is expressed as follows:

$$373 T_{ice}^{i+1} = C_{gr\_ice} + D_{gr\_ice} \cdot T_{ice}^i \quad (27)$$

374 Similarly to the snow coefficients (see Eqs 20 and 21),  $\lambda_{ice}$ ,  $C_{gr\_ice}$ ,  $D_{gr\_ice}$  depend on the vertical discretization  
375 and the thermal properties of the ice. The formulations of the heat capacity ( $C_{ice}$ ) and thermal conductivity ( $\lambda_{ice}$ )  
376 of the ice have been taken from those used in the GRISLI ice-sheet model (Yen, 1981) and are given by:

$$377 C_{ice} = \rho_{ice} (a_{ci} + b_{ci} (T_{ice} - T_0)) \quad (28)$$

$$378 \lambda_{ice} = a_{\lambda i} \exp(b_{\lambda i} \times T_0) \quad (29)$$

379 where  $T_{ice}$  is the ice temperature,  $a_{ci} = 2115.3 \text{ J K}^{-1} \text{ kg}^{-1}$ ,  $b_{ci} = 7.79293 \text{ J K}^{-2} \text{ kg}^{-1}$ ,  $a_{\lambda i} = 6.727 \text{ W m}^{-1} \text{ K}^{-1}$  and  $b_{\lambda i}$   
380  $= -0.041 \text{ K}^{-1}$ .

381 A major difference between the hydrology of snow and ice layers lies in the fact that ice is considered as an  
382 impermeable medium. Hence, liquid water coming from melting ice is considered to runoff instantaneously with  
383 no possibility of refreezing. As a result, when the ice temperature is above the melting point, the available energy  
384 for phase change in the  $i^{\text{th}}$  ice layer ( $\text{J m}^{-2}$ ) is given by:

$$385 E_{ice}^i = C_{ice}^i (T_{ice}^i - T_0) D_{ice}^i \quad (30)$$

386 Similarly to  $S_{melt}$  (Eq. 24), the total amount of ice melt is given by:



387 
$$I_{melt} = \frac{\sum_t E_{ice}^i}{L_f} \quad (31)$$

388 and the runoff is computed as the sum of  $S_{melt}$  and  $I_{melt}$ . Given the fact that snow drift is ignored, the surface  
389 mass balance is computed as:

390 
$$SMB = P_{snow} + P_{rain} - S_{melt} - I_{melt} - S_{snow} \quad (32)$$

### 391 2.2.3 Other processes in the new ES model

392 Another modification made to the ES module concerns the inclusion of rainwater percolation within the snowpack  
393 that may refreeze at depth as long as the maximum water holding capacity is not exceeded. To account for the  
394 darkening effect (i.e., lower albedo) due to dust deposition with liquid precipitation, we also enhanced snow ageing  
395 by a factor of two in case of a rainfall event.

396 The snow thermal conductivity has been modified to follow a similar formulation to that used in the ISBA-ES  
397 model (Decharme et al., 2016) and the CROCUS model (Vionnet et al., 2012) and early proposed by Yen (1981).  
398 Therefore, the effective thermal conductivity in the  $i^{th}$  layer now reads as:

399 
$$\Lambda_{eff}^i = \left( a_{\lambda v} + \frac{b_{\lambda v}}{c_{\lambda v} + T_{snow}^i} \right) \frac{P_0}{P} + \Lambda_{ice} \left( \frac{\rho_s^i}{\rho_w} \right)^{1.88} \quad (33)$$

400 The first term of the right-hand side that parameterizes the water vapor diffusion effects ( $\Lambda_{vap}^i$ ) remains unchanged  
401 (see Eq. 15). The second term replaces Eq. (14) used in the previous ES version (Wang et al. 2013) and corresponds  
402 to the new formulation of the snow thermal conductivity ( $\Lambda_{cond}^i$ ). Here, the ice thermal conductivity ( $\Lambda_{ice}$ ) differs  
403 from the value found in Decharme et al. (2016) and is given by Eq. (29).

404 Besides the new snow layering scheme and the changes mentioned in this section, all the other processes simulated  
405 in the new ES module are treated in the same way as in the three-layer version.

## 406 3. Experimental setup

### 407 3.1 Forcing by the regional atmospheric model MAR

408 The ORCHIDEE-ICE simulations presented in this paper were driven by the atmospheric outputs of the regional  
409 atmospheric model MAR (Fettweis et al., 2017). This approach was motivated by the fact that MAR was initially  
410 developed for polar regions (Gallée and Schayes, 1994). Moreover, it is coupled to a land surface scheme, SISVAT  
411 (Soil Ice Snow Vegetation Atmosphere Transfer, De Ridder and Schayes, 1997), that includes a physically-based  
412 snowpack model derived from the multi-layered snow model CROCUS (Brun, 1989, 1992). As such, MAR has  
413 been extensively used to simulate the present-day climate and surface mass balance of the GrIS, and compares  
414 well to reanalyses and available data of SMB measurements (e.g., Fettweis et al. 2017, 2020; Franco et al. 2012;  
415 Montgomery et al. 2020; Delhasse et al., 2020). Therefore, the use of atmospheric forcings from MAR offers a  
416 good opportunity to assess the performances of our snow model for simulating the SMB and ablation-related  
417 processes.

418 The MAR simulations (1960 – 2019) were run at a 20 km x 20 km resolution. Here, we use the version v3.11.4,  
419 identical to the version v3.11.5 for the Greenland ice sheet (Smith et al. 2023). MAR was forced every six hours  
420 at its lateral boundaries by the meteorological fields (temperature, humidity, wind, and pressure) coming from the



421 ERA-40 (1960-1978, Uppala et al., 2005) and the ERA-Interim (1979-2019, Dee et al., 2011) reanalyses from the  
422 European Centre for Medium-Range Weather Forecasts (ECMWF). Sea surface temperatures and sea ice cover,  
423 also coming from ECMWF reanalyses, were 6-hourly prescribed.

### 424 3.2. The ORCHIDEE-ICE simulations

425 The ORCHIDEE-ICE simulations are run at a half-hourly time step with the same spatial resolution as the MAR  
426 outputs (20 km x 20 km). The integration domain covers the whole of Greenland. ORCHIDEE-ICE is forced every  
427 three hours by the downward shortwave and longwave radiation, the surface air temperatures and specific humidity  
428 (all at 2 meters) and the wind speed (at 10 meters), the surface pressure and the precipitation rate (split between  
429 rainfall and snowfall). Simulations are performed over the 1995-2019 period. The first five years (1995 to 1999)  
430 are used for the initialization of the snowpack and are not included in the analysis. However, to obtain reasonable  
431 thermal conditions within the ice layers, a longer time integration is required. Thus, we performed a preliminary  
432 spin-up experiment over the same 25 years to infer an initial vertical temperature profile for the subsequent  
433 ORCHIDEE-ICE simulations.

434 The name and the characteristics of the different experiments presented in this paper are summarized in Table 1.  
435 Using the experimental design described above, we first ran the ES model with three and twelve snow layers (STD-  
436 3L and STD-12L experiments respectively) to evaluate the added value of the new layering scheme. These  
437 experiments were carried out with the albedo parameters used in the CMIP6 ORCHIDEE version (Chéruy et al.,  
438 2020) and referred hereafter to as the standard snow albedo parameters.

439 Due to the strong sensitivity of the SMB to the albedo, we also conducted two additional experiments with  
440 modified values of the albedo parameters. In the ASIM-12L experiment, we used the parameters inferred from the  
441 approach of Raoult et al. (2023). This latter was based on a data assimilation experiment using the MODIS  
442 retrievals. The main goal of their study was to optimise the albedo parameters so as to improve the albedo for the  
443 ice sheet as a whole, while giving an extra weight to the edges where the greatest amount of runoff is produced.  
444 In doing this, they also succeeded in improving the model-data fit over the whole GrIS by reducing the root-mean-  
445 square error (RMSE) by ~22 %. However, their work was done with a previous version of the ORCHIDEE-ICE  
446 model with only three snow layers and in which the ice layers were not implemented. Instead, ice was mimicked  
447 by a soil type whose porosity and volumetric water content were set to 98% to simulate a soil filled with frozen  
448 water.

449 The logical follow-up to the work of Raoult et al. (2023) would have been to apply the optimisation algorithm to  
450 the new version of ORCHIDEE-ICE. Since this approach is highly time-consuming, it has not yet been carried  
451 out, albeit it will be the focus of further investigations. Therefore, using the new ORCHIDEE-ICE model version,  
452 we adopted a manual tuning approach (i.e., trial and error method) to adjust the albedo parameters (OPT-12L  
453 experiment). This procedure consists in 1/ changing the parameter values, the new value being taken from the  
454 range reported in Table 1, 2/ running the model with the new parameter values, 3/ evaluating the model  
455 performance using statistical criteria (e.g. RMSE) and 4/ repeating steps 1/ to 3/ until an acceptable calibration is  
456 obtained.

457 Finally, to assess the impact of the climatic fields used as inputs of ORCHIDEE-ICE, we performed another  
458 experiment (ERA5-12L experiment) by forcing the model with the ERA5 reanalysis (Hersbach et al., 2020) and  
459 using the same albedo parameters than in OPT-12L experiment.



460 **Table 1:** List of the ORCHIDEE-ICE experiments (first column) with values chosen for the different albedo  
 461 parameters (standard albedo parameters for STD-3L and STD-12L, optimized albedo parameters inferred from  
 462 Raoult et al. (2023) for ASIM-12L and manual-tuned parameters for OPT-12L and ERA-12L. Values in brackets  
 463 indicate for each parameter the range of values considered in the manual tuning approach.

| Exp.           | Nb of snow layers | $A_{aged}$<br>[0.50 - 0.70] | $B_{dec}$<br>[0.10 - 0.40] | $\tau_{dec}$<br>[1.0 - 10.0] | $\delta_c$<br>[0.2 - 2.0] | $\omega_1$<br>[1.0 - 7.0] | $\omega_2$<br>[0.5 - 6.0] | $\tau_{max}$<br>[40 - 60] | $\alpha_{ice}$<br>[0.30 - 0.50] |
|----------------|-------------------|-----------------------------|----------------------------|------------------------------|---------------------------|---------------------------|---------------------------|---------------------------|---------------------------------|
| STD-3L         | 3                 | 0.620                       | 0.170                      | 10                           | 0.2                       | 7                         | 4                         | 50                        | 0.400                           |
| STD-12L        | 12                | 0.620                       | 0.170                      | 10                           | 0.2                       | 7                         | 4                         | 50                        | 0.400                           |
| ASIM-12L       | 12                | 0.553                       | 0.320                      | 6.911                        | 0.783                     | 3.037                     | 3.974                     | 56.183                    | 0.476                           |
| <b>OPT-12L</b> | <b>12</b>         | <b>0.580</b>                | <b>0.280</b>               | <b>2.0</b>                   | <b>1.0</b>                | <b>3</b>                  | <b>6</b>                  | <b>54</b>                 | <b>0.420</b>                    |
| ERA-12L        | 12                | 0.580                       | 0.280                      | 2.0                          | 1.0                       | 3                         | 6                         | 54                        | 0.420                           |

464

#### 465 4. Methodology for the model performance evaluation

##### 466 4.1 Comparison with MAR outputs

467 Our first objective is to assess the performance of the ORCHIDEE ICE model in representing the GrIS SMB. The  
 468 period under study spans over the 2000-2019 period. As mentioned in Section 3, MAR has revealed good  
 469 capabilities in simulating the SMB of present-day Greenland when compared to observational data. Therefore, at  
 470 the scale of the entire GrIS, our evaluation is made with respect to the MAR outputs (Figs 2a-5a). In all simulations  
 471 presented in this paper except ERA5-12L, the forcing fields of the ORCHIDEE-ICE model are provided by MAR  
 472 outputs. These include solid and liquid precipitation which constitute the accumulation (and the climatic)  
 473 component of the SMB. By using the MAR forcing, our analysis of the ability of ORCHIDEE-ICE to reproduce  
 474 ablation processes (runoff and sublimation) is made simpler and is not biased by the use of another forcing.

##### 475 4.2 MODIS

476 In this study, we compared the albedo computed in ORCHIDEE-ICE with satellite-derived estimates of daily  
 477 albedo. We used Collection 6 from the MOD10A1 product (Hall et al., 1995) retrieved from the NASA space-  
 478 borne sensor MODIS. We chose this product because it has a good spatiotemporal coverage over snow-covered  
 479 areas. It is also one of the best performing products in terms of comparison with in situ data (Urraca et al., 2022,  
 480 2023). Moreover, while studies based on the previous Collection 5 reported deficiencies at latitudes higher than  
 481 70°N (Alexander et al., 2014), substantial improvements have been made to Collection 6 by using all available  
 482 observations for the acquisition period against only four observations per day in Collection 5  
 483 (<https://lpdaac.usgs.gov/products/mcd43d11v006/>, last access 01/22/2024). As a result, better quality retrievals are  
 484 obtained at high latitudes despite a slight negative bias (Urraca et al., 2022). To avoid inaccuracies in retrieved  
 485 data due to the presence of clouds or aircraft condensation trails, the MOD10A1 albedo product used in this study  
 486 was further processed by Box et al. (2017): data have been de-noised, gap-filled, corrected for the sun-angle bias  
 487 and validated using daily ground albedo values from the PROMICE (Programme for Monitoring of the Greenland  
 488 ice sheet, Fausto et al., 2021) and GC-net automatic weather stations (Box et al. 2017).



489 We aggregated the albedo data (500 m x 500 m) onto the MAR grid to make the comparison between MODIS data  
490 and the ORCHIDEE-ICE outputs. In this study, we used the albedo data covering the 2000-2017 period because  
491 data for the years 2018 and 2019 were undefined. The resulting dataset may be used to calibrate the mean  
492 ORCHIDEE-ICE albedo, computed as the mean between the visible (from 0.4 to 0.7  $\mu\text{m}$ ) and near infrared (from  
493 0.7 to 2.5  $\mu\text{m}$ ) bands (see Section 2).

## 494 5. Results

### 495 5.1 Evaluation against MAR for standard albedo parameters

496 Figures 2 to 4 display the spatial distribution of the runoff, sublimation and refreezing simulated by MAR (panels  
497 a) and by ORCHIDEE-ICE in the STD-3L (panels b) and STD-12L (panels c) experiments.

498 The main runoff areas simulated with MAR are located on the western edge albeit, to some extent, runoff occurs  
499 in all peripheral areas of the ice sheet (Fig. 2a). Locations of the ablation zones are well represented in  
500 ORCHIDEE-ICE but are limited to a very narrow band, especially in the STD-3L simulation (Fig. 2b). Increasing  
501 the number of snow layers favors the inland expansion of the ablation areas on the western and northern margins  
502 (Fig. 2c). However, this expansion remains too restricted compared to MAR (Fig. 2a). Integrated over the whole  
503 ice sheet (Table 2), the runoff values computed in STD-3L (152 Gt yr<sup>-1</sup>) and STD-12L (205 Gt yr<sup>-1</sup>) experiments  
504 for the 2000-2019 period are respectively 59 % and 45 % lower compared to MAR (375 Gt yr<sup>-1</sup>). As a consequence  
505 of the considerably smaller amount of runoff in ORCHIDEE-ICE, and thus of surface meltwater, refreezing is also  
506 much lower (Table 2) and less extended (Figs. 3a-c) compared to MAR.

507

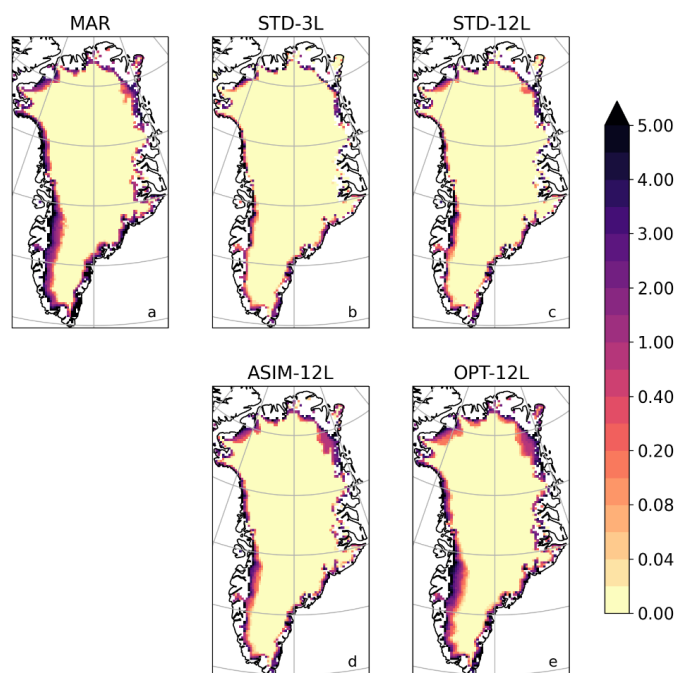
508

509





Runoff 2000-2019 ( $\text{mm day}^{-1}$ )



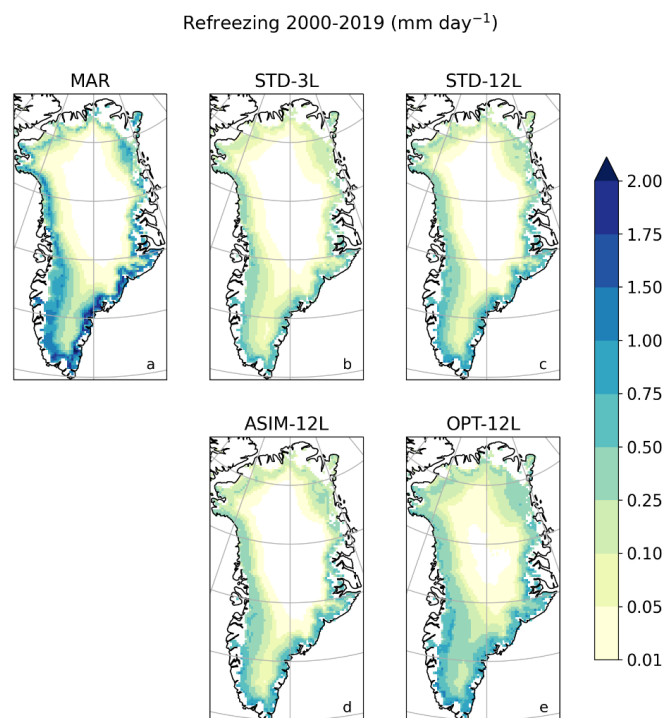
510

511 **Figure 2:** Spatial distribution of the runoff (in  $\text{mm day}^{-1}$ ) averaged over the 2000-2019 period and simulated with  
 512 MAR (a) and the ORCHIDEE-ICE model (b-e) using: the three-layer snow scheme and the standard albedo  
 513 parameters (b), the twelve-layer snow scheme and the standard albedo parameters (c), the twelve-layer snow  
 514 scheme and the albedo parameters optimised using a data assimilation technique (Raoult et al., 2023) and a  
 515 previous version of the ORCHIDEE-ICE model (d), the twelve-layer snow scheme and the albedo parameters  
 516 obtained after manual tuning.

517

518 **Table 2:** Simulated values of SMB, runoff, sublimation and refreezing integrated over the entire Greenland ice  
 519 sheet and averaged over the 2000-2019 period. Values in brackets indicate the root-mean-square error with respect  
 520 to MAR outputs.

| Experiments    | SMB ( $\text{Gt yr}^{-1}$ )<br>[RMSE w.r.t. MAR,<br>in $\text{m yr}^{-1}$ ] | Runoff ( $\text{Gt yr}^{-1}$ )<br>[RMSE w.r.t. MAR,<br>in $\text{m yr}^{-1}$ ] | Sublimation ( $\text{Gt yr}^{-1}$ )<br>[RMSE w.r.t. MAR,<br>in $\text{m yr}^{-1}$ ] | Refreezing ( $\text{Gt yr}^{-1}$ )<br>[RMSE w.r.t. MAR,<br>in $\text{m yr}^{-1}$ ] |
|----------------|---|--|---|--|
| <b>MAR</b>     | <b>286</b>  | <b>375</b>   | <b>82</b>   | <b>186</b>   |
| STD-3L         | 504 [0.356]   | 152 [0.404]  | 33 [0.036]  | 72 [0.123]   |
| STD-12L        | 450 [0.287]   | 205 [0.337]  | 33 [0.035]  | 104 [0.098]  |
| ASIM-12L       | 453 [0.276]   | 220 [0.324]  | 15 [0.044]  | 97 [0.103]   |
| <b>OPT-12L</b> | <b>301 [0.169]</b>  | <b>336 [0.216]</b>   | <b>52 [0.028]</b>   | <b>158 [0.087]</b>   |
| ERA5-12L       | 352   | 273  | 89  | 141  |



521

522 **Figure 3:** Same as Figure 2 for the simulated refreezing (in  $\text{mm day}^{-1}$ ).

523 Large differences between MAR and ORCHIDEE-ICE also arise regarding sublimation ( $32$  and  $33 \text{ Gt yr}^{-1}$  in the  
524 STD-3L and STD-12L experiments respectively, against  $82 \text{ Gt yr}^{-1}$  for the 2000-2019 period in MAR). This feature  
525 concerns the entire ice sheet but is even more striking in peripheral areas and, to a lesser extent, in central  
526 Greenland where condensation occurs (Fig. 4).

527 The differences in simulated runoff and in sublimation between MAR and ORCHIDEE-ICE translate into  
528 overestimated SMB values simulated with ORCHIDEE-ICE ( $504$  and  $450 \text{ Gt yr}^{-1}$  in STD-3L and STD-12L against  
529  $286 \text{ Gt yr}^{-1}$  in MAR; see also Fig. 5). Since inland regions are dominated by the accumulation signal, which is  
530 provided by the MAR outputs, the SMB anomalies are primarily driven by differences in the ablation components  
531 occurring at the edges of the ice sheet, and exceed  $2 \text{ m yr}^{-1}$  in most parts of the western and southeastern margins.

532 An important conclusion that can be drawn from these results is that the use of a better resolved snow layering  
533 scheme (twelve-layer as opposed to a three-layer snow scheme) reduces the mismatch between MAR and  
534 ORCHIDEE-ICE. This is illustrated by the integrated SMB and runoff values which are respectively  $\sim 35\%$  higher  
535 and  $\sim 11\%$  lower in STD-12L, translating into reductions of RMSE values ( $\sim 19\%$  and  $\sim 17\%$  for SMB and runoff  
536 respectively, see Table2). Nevertheless, the differences with MAR are still too large for the model to be used as a  
537 reliable tool to compute the GrIS SMB.

538

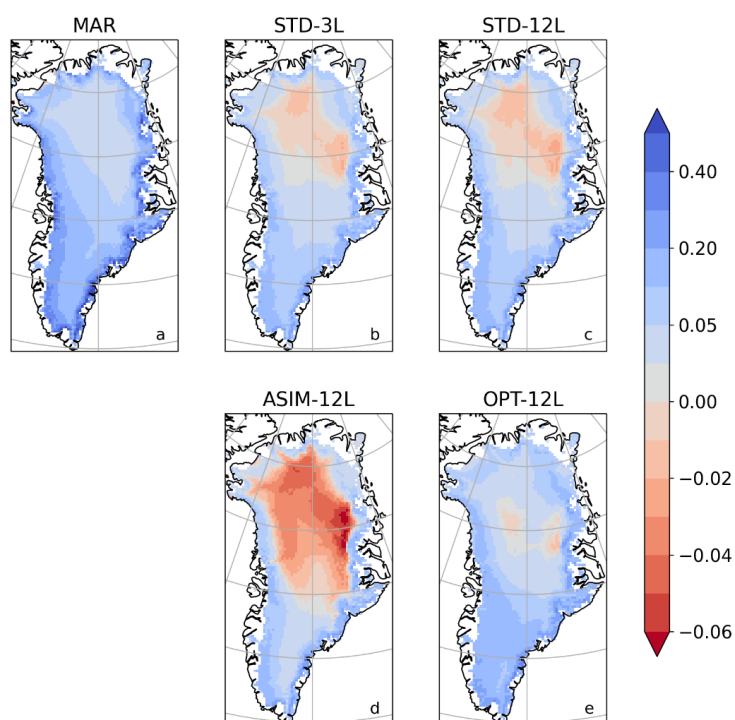
539

540

541



Sublimation 2000-2019 ( $\text{mm day}^{-1}$ )



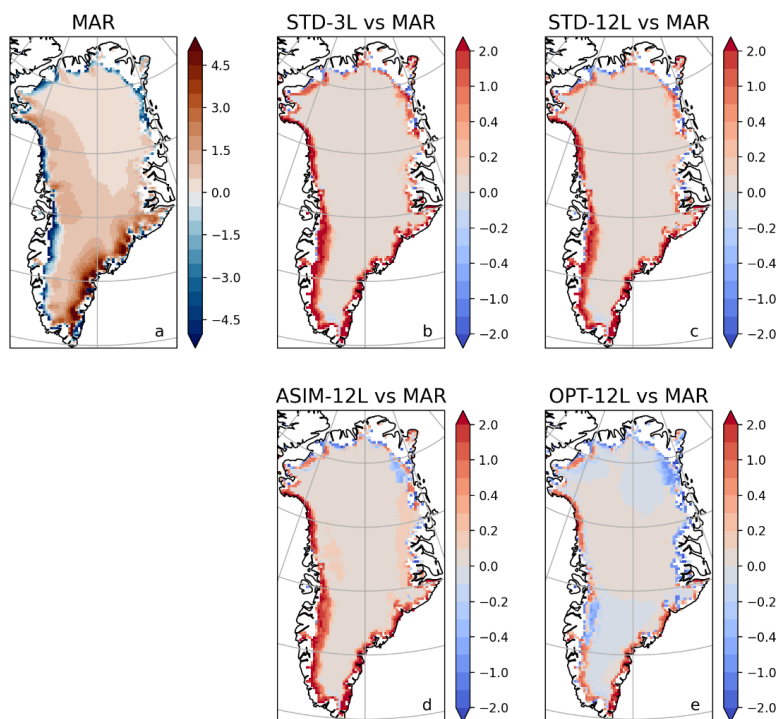
542

543 **Figure 4:** Same as Figure 2 for the simulated sublimation (in  $\text{mm day}^{-1}$ ). Negative values indicate condensation.

544



SMB differences 2000-2019 ( $\text{mm day}^{-1}$ )



545

546 **Figure 5:** Spatial distribution of the GrIS SMB simulated with MAR (in  $\text{mm day}^{-1}$ ) and averaged over the 2000-  
547 2019 period (a) Differences in the GrIS surface mass balance between MAR and the ORCHIDEE-ICE model (b-  
548 e) with the standard parameter values of the albedo parameterisation and the three-snow layering scheme (b).  
549 Panels (c-e) correspond to simulations performed with the updated twelve-snow layering scheme for standard  
550 values of the albedo parameters (c), optimised values of the albedo parameters (d), values of the albedo parameters  
551 obtained after manual tuning (e).

## 552 5.2. SMB and runoff for modified albedo parameters

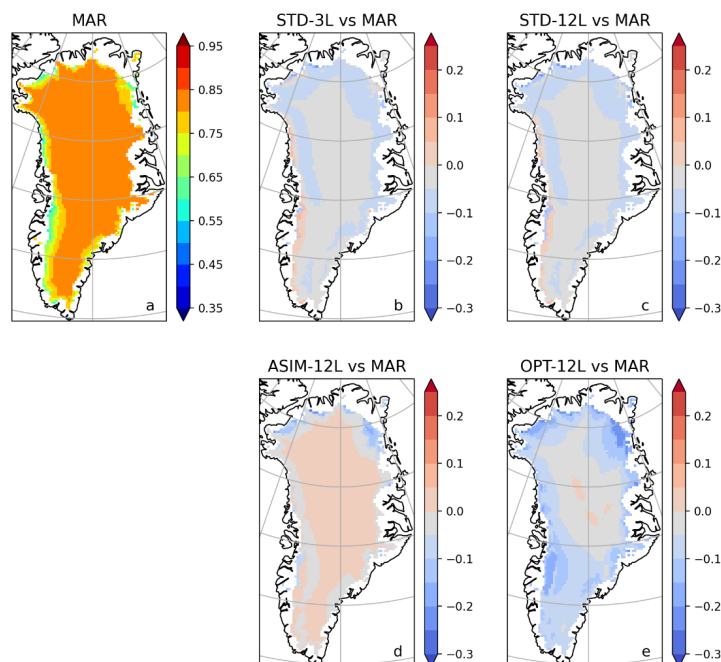
### 553 5.2.1 Impact of optimised albedo parameters

554 As snow is a highly reflective medium, little changes in albedo may produce large changes in the surface energy  
555 budget, and thus, in the SMB. In the GrIS interior, there is generally a broad agreement between the summer albedo  
556 computed by MAR and the standard ORCHIDEE-ICE simulations (i.e. STD-3L and STD12-L experiments, Figs.  
557 6b and 6c). Slight negative anomalies ( $\sim -0.05$ ) appear, mainly in the northern part of the ice sheet, but with only  
558 little consequences on surface melting owing to the very cold conditions in this region. However, on the western  
559 margin, where most of the melting takes place, larger snow albedo values are found in ORCHIDEE-ICE. This  
560 leads to underestimated surface temperatures compared to MAR (Fig. 7) and, thus, to undervalued runoff that may  
561 explain part of the discrepancies between MAR and ORCHIDEE-ICE. There are also differences between the  
562 observations provided by MODIS retrievals and the MAR albedo (Figs. 8a, 8b), especially in the northern and  
563 southern parts, and the western margin. On the other hand, the summer albedo computed in the STD-3L and STD-



564 12L experiments (Figs. 8c, 8d) are generally too low in the interior of the ice sheet, and too high on the western  
565 margin with differences from 0.05 to 0.15.  
566

Summer Albedo differences with MAR 2000-2017



567

568 **Figure 6:** Spatial distribution of the summer albedo computed with MAR and averaged over the 2000-2017 period  
569 (a) and differences between the albedo computed with ORCHIDEE-ICE and MAR for the three-layer snow scheme  
570 and the standard albedo parameters (b), the twelve-layer snow scheme and the standard albedo parameters (c), the  
571 albedo parameters inferred from a data assimilation technique and using a previous version of the ORCHIDEE-  
572 ICE model (d), the albedo parameters obtained after manual tuning (e).

573 As mentioned in Section 3.2, we investigated the sensitivity of the SMB and its components on the albedo. We  
574 first performed an ORCHIDEE-ICE experiment (ASIM-12L) with the optimised albedo parameters inferred from  
575 Raoult et al. (2023). Figure 8e illustrates how the representation of the albedo has been improved in the ASIM-  
576 12L experiment compared to STD-12L (Fig. 8d). Model-data discrepancies are now reduced with differences  
577 lower than 0.05 except in the northernmost parts of the ice sheet. In addition, the RMSE decreased by ~24 %  
578 (Table 3), which is consistent with Raoult et al. (2023). The ablation areas are now better represented (Fig. 2d)  
579 due to increased surface temperatures (Fig. 7c) as a result of lower albedo values on the western margin (Fig. 8d).  
580 However, despite the smaller mismatch between modeled albedo and MODIS retrievals and the better  
581 representation of the ablation areas, the simulated amount of runoff ( $220 \text{ Gt yr}^{-1}$ ) integrated over the whole GrIS  
582 has been only slightly improved with respect to STD-12L (Figs. 2d) and remains quite different from MAR outputs  
583 (Figs. 2a), and the simulated SMB ( $453 \text{ Gt yr}^{-1}$ ) has even been slightly degraded (Figs. 5a and 5d) due to strong  
584 negative temperature anomalies in central Greenland (Fig. 7c). These unsatisfactory results could be explained by

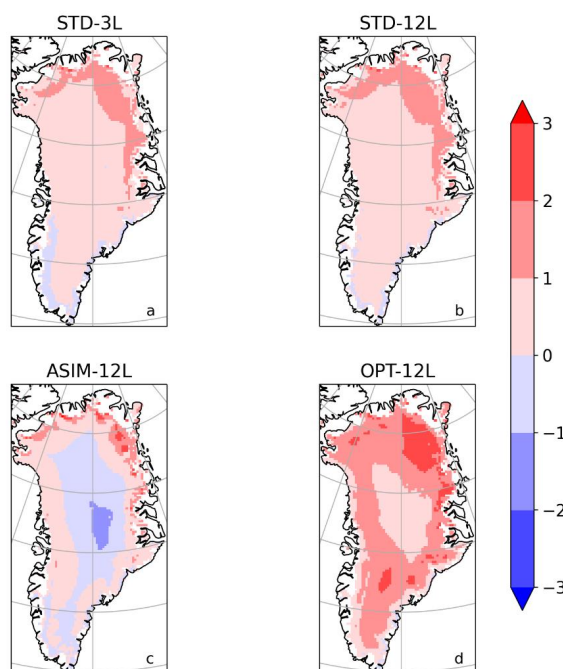


585 the use of an earlier version of the ORCHIDEE-ICE model to perform the optimisation, in which ice layers were  
586 not implemented, likely causing an underestimation of runoff.

587

588

Summer snow surface temperature differences with MAR



589

590 **Figure 7:** Spatial distribution of the snow temperature differences with respect to MAR averaged over the 2000-  
591 2019 period (in °C) simulated for the STD-3L (a), STD-12L (b), ASIM-12L (c) and OPT-12L (d) experiments.

592 The low performance for the SMB computation in ASIM-12L is not solely due to a small amount of runoff but  
593 also to strong negative values of sublimation (i.e., large condensation) over central Greenland (Fig. 3d) resulting  
594 in an average level of 15 Gt yr<sup>-1</sup> over the entire ice sheet compared to 82 Gt yr<sup>-1</sup> in MAR (Table 2). In the ASIM-  
595 12L experiment, the albedo in the central GrIS region is slightly higher (up to 0.05) than the albedo retrieved from  
596 MODIS (Fig. 8e), while the albedo computed with MAR is slightly lower (Fig. 8b). This explains why the ASIM-  
597 12L surface temperatures are smaller than those simulated with MAR. This can lead therefore to lower saturation  
598 pressures that can drop below the dew point and thus produce solid condensation. This result highlights the key  
599 influence of the albedo on surface processes and, in particular, illustrates how a small departure from observations  
600 may lead to strong biases in sublimation estimates.

### 601 5.2.2 Manual tuning

602 As mentioned in Section 3, we have not yet performed a data assimilation experiment to calibrate the new twelve-  
603 layer ES model, given the computational cost of such an experiment. Instead, we chose to follow a trial and error  
604 approach. As runoff dominates the SMB signal, our primary objective was to improve the runoff computation by



605 reducing the summer albedo values in the main ablation areas (i.e., the western margin). Given the number of  
606 albedo parameters, several options are available to achieve this:

- 607 • lowering the albedo of aged snow ( $A_{aged}$ ) and/or the albedo of fresh snow ( $A_{aged} + B_{dec}$ );
- 608 • modifying the parameter controlling the decay rate of snow albedo ( $\tau_{dec}$ );
- 609 • increasing snow age by changing the parameters related to snow aging: the minimum snowfall thickness  
610 to reset snow age to zero ( $\delta_c$ ), the tuning parameters  $\omega_1$ ,  $\omega_2$  (see Eq. 10) and the maximum snow age  
611 ( $\tau_{max}$ );
- 612 • changing the ice albedo ( $\alpha_{ice}$ ) because it can also affect SMB and runoff computation if the snowpack  
613 melts entirely during summer months in some places and give rise to bare ice.

614 Owing to the various influences of the albedo parameters, we had to find a compromise so as to lower the albedo  
615 in ablation areas and improve the computation of runoff and SMB, while keeping reasonable albedo values in the  
616 GrIS interior. Among the values we tested for each of the parameters, the set of parameters providing the best  
617 agreement with MAR outputs (for SMB and SMB components) is highlighted in bold in Table 1 (OPT-12L  
618 experiment). Compared to the ASIM-12L experiment (Fig. 8e), the albedo mismatch between ORCHIDEE-ICE  
619 (OPT-12L experiment) and MODIS is amplified, especially along the western margin and in the northern sector  
620 with differences reaching 0.25 and 0.3 respectively (Fig. 8f). Nevertheless, these results were expected since our  
621 manual tuning was designed to increase the magnitude of the ablation components (especially runoff) and to  
622 decrease the SMB, and therefore to lower the albedo values with a direct impact on surface temperatures, hence  
623 surface melting and sublimation.

### 624 **5.2.3 Impact on SMB components**

625 Using the new set of albedo parameters obtained with the manual tuning approach, the ablation areas are now  
626 much more extended than those simulated in the STD-12L experiment (Figs. 2c and 2e). Compared to MAR (Fig.  
627 2a), they are even wider in the northern part due to increased surface temperatures (Fig. 7d) in response to lower  
628 albedo values (up to -0.25). The total amount of runoff averaged over the 2000-2019 period is now 336 Gt yr<sup>-1</sup>  
629 (against 375 Gt yr<sup>-1</sup> in MAR). For the OPT-12L experiment, the RMSE value has decreased by ~40% compared  
630 to STD-12L (Table 2), meaning that the improvement in the runoff computation over the whole of GrIS does not  
631 result from compensation biases. In the same way, the sublimation (52 Gt yr<sup>-1</sup>) and refreezing (158 Gt yr<sup>-1</sup>) better  
632 match with MAR (Table 2). In particular, condensation over central Greenland has been considerably reduced,  
633 notably with respect to ASIM-12L, but sublimation is still underestimated along the GrIS edges and in the southern  
634 part (Fig. 4e). The increase in refreezing (with respect to STD-12L and ASIM-12L) in the GrIS interior (Fig. 3e)  
635 is likely linked to lower summer albedo values (Figs. 6e, 8f) leading to a smaller amount of melting compensated  
636 by refreezing. In the main ablation areas, a larger refreezing is produced and thus a better agreement with MAR,  
637 though still insufficient, is obtained.

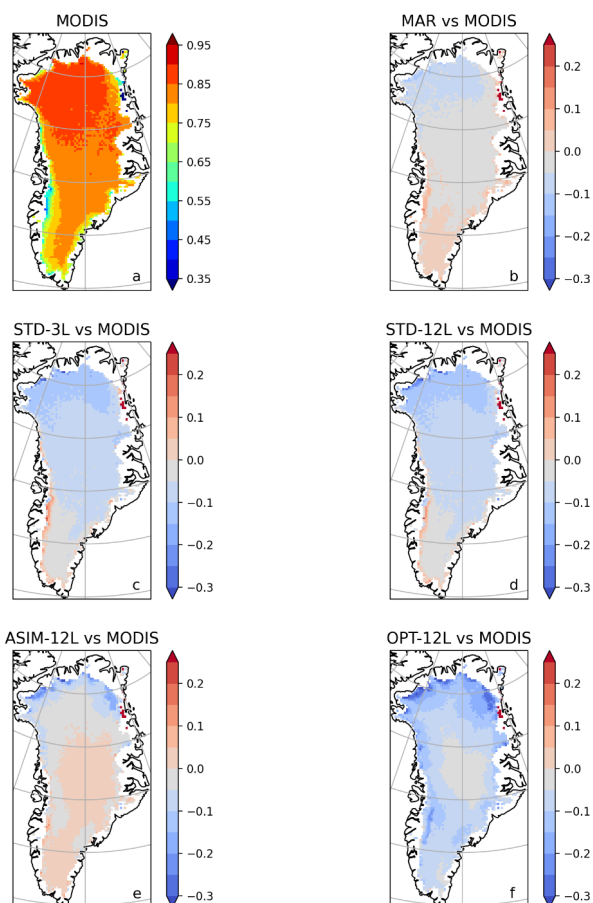
638 These results for the SMB components are evidently associated with an improved representation of the SMB itself  
639 (Fig. 5e) which now reaches 301 Gt yr<sup>-1</sup> (286 Gt yr<sup>-1</sup> obtained with MAR), and with a ~41% decrease in the RMSE  
640 value compared to STD-12L (Table 2).

641

642



### Summer Albedo differences with MODIS 2000-2017



643

644 **Figure 8:** Spatial distribution of the MODIS summer albedo averaged over the 2000-2017 period (a) and  
645 differences between the albedo computed with MAR and MODIS (b), and with ORCHIDEE-ICE and MODIS for  
646 the three-layer snow scheme and the standard albedo parameters (c), the twelve-layer snow scheme and the  
647 standard albedo parameters (d), the albedo parameters inferred from a data assimilation technique and using a  
648 previous version of the ORCHIDEE-ICE model (e), the albedo parameters obtained after manual tuning (f).

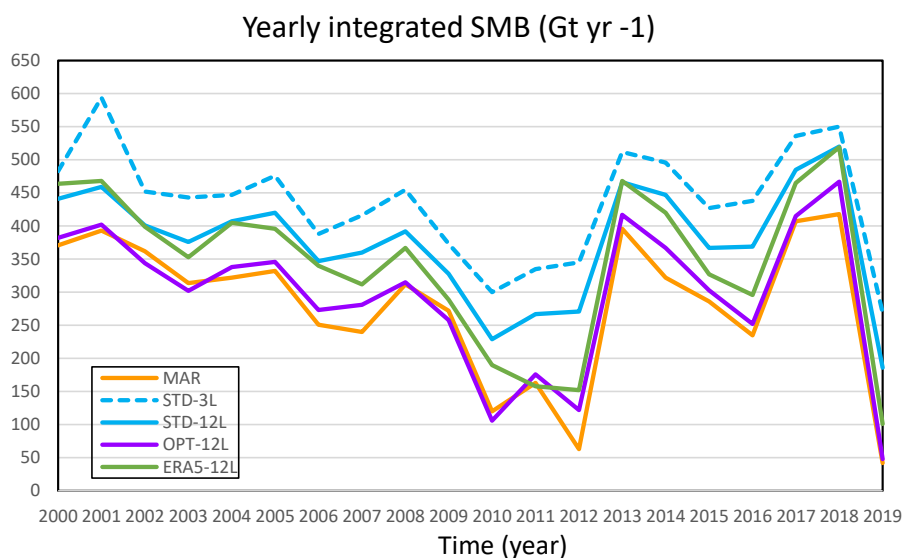
### 649 5.3 SMB evolution: impact of the climate forcing

650 The results presented in the previous sections were averaged over the 2000-2019 period (for SMB and the SMB  
651 components) and over the 2000-2017 period (for the albedo). In this part, we present the temporal evolution of the  
652 SMB between years 2000 and 2019 (Fig. 9). Figure 8 shows that whatever the ORCHIDEE-ICE experiment under  
653 consideration, the evolution of the yearly integrated SMB is in accordance with the evolution simulated by the  
654 MAR model. In particular, the years in which extreme melting events were recorded (such as 2012 and 2019) are  
655 perfectly well represented (Bennartz et al. 2013; Tedesco and Fettweis 2020). As expected, the best agreement  
656 with MAR is obtained for the OPT-12L experiment as a result of the calibration of the albedo parameters.





657 When forced by the ERA-5 meteorological fields, and using the manually-tuned parameters, ORCHIDEE-ICE  
658 simulates higher SMB values and a lower runoff (Fig. 9 and Table 2), especially during the first period of the time  
659 series (2000-2008). However, the evolution of the yearly integrated SMB in the ERA5-12L experiment follows  
660 exactly the same interannual variations as for the OPT-12L experiment forced with MAR (Fig. 9). This indicates  
661 that the surface climate simulated by MAR is close to that derived from the ERA-5 products. Moreover, in a  
662 comparative study of the ERA-5 reanalyses, Arctic System reanalysis and MAR performances, Delhasse et al.  
663 (2020) showed that MAR outperforms ERA-5 for the near-surface temperatures when compared to observations  
664 from automatic weather stations. As the surface melt, and thus the SMB, largely depend on near-surface  
665 temperatures, there is therefore a strong interest in using MAR to force our snow model and to compare its  
666 performances to those of MAR.  
667



668  
669 **Figure 9:** Evolution of the yearly surface mass balance of the Greenland ice sheet simulated with MAR (black),  
670 ORCHIDEE-ICE forced by MAR outputs (STD-3L and STD-12L: yellow, solid and dashed lines respectively;  
671 OPT-12L: red line), ORCHIDEE-ICE forced by the ERA-5 reanalyses (green line).

## 672 6. Discussion and concluding remarks

673 The land surface component of the IPSL ESM used for CMIP6 included a three-layer snowpack model operating  
674 over continental surfaces. However, this snow scheme was not adapted to glaciated surfaces, which is a major  
675 drawback and makes it impossible to compute the surface mass balance over ice sheets or glaciers. The aim of this  
676 paper was therefore to present the new developments made to adapt the snow model to ice-covered areas and to  
677 document its performance. Our first step was to calibrate the snow albedo parameterisation over the Greenland ice  
678 sheet. To have a set of climate variables covering the whole ice sheet, we chose to force our model by the  
679 atmospheric outputs of the MAR regional model which shows very good performances to simulate the surface  
680 climate and thus offers undeniable advantages for the representation of the physical processes related to snow and  
681 ice, in particular surface melting (Delhasse et al., 2020). We have shown that the ablation-related processes are



682 highly dependent on the choice of the albedo parameters. The set of parameters obtained after manual tuning (OPT-  
683 12L experiment) provides a good agreement between the SMB computed in ORCHIDEE-ICE and MAR.  
684 However, the summer albedo computed with this set of parameters has been degraded compared to MAR and  
685 MODIS and to the albedo computed in the ASIM-12L experiment (based on the MODIS-optimised albedo  
686 parameters) as shown in Table 3 and in Figures 6d,e and 7e,f. While the RMSEs computed between ORCHIDEE-  
687 ICE and MAR for SMB and runoff have been reduced by ~39% and ~33% respectively from ASIM-12L to OPT-  
688 12L, the RMSE for albedo has increased by 47% (Table 3). The mismatch between MODIS retrievals and OPT-  
689 12L albedo is mainly observed in the northernmost part of the ice sheet and, to a lesser extent, on the western  
690 edge.

691 **Table 3:** Albedo RMSE values between MAR and MODIS (first line), between ORCHIDEE-ICE and MODIS  
692 (second column) and between ORCHIDEE-ICE and MAR (third column).

| Experiments | RMSE<br>(w.r.t MODIS) | RMSE<br>(w.r.t MAR) |
|-------------|-----------------------|---------------------|
| MAR         | 0.076                 |                     |
| STD-3L      | 0.098                 | 0.055               |
| STD-12L     | 0.097                 | 0.058               |
| ASIM-12L    | 0.076                 | 0.045               |
| OPT-12L     | 0.111                 | 0.092               |

693  
694 A more objective method would be to perform a data assimilation experiment similar to the one presented in Raoult  
695 et al. (2023) using the new version of the ORCHIDEE-ICE model. However, albedo is not the only important  
696 parameter governing the snowpack evolution. The albedo parameters inferred from Raoult et al. (2023)'s  
697 optimisation greatly improve the representation of the albedo, but degrade the other model outputs compared to  
698 those obtained with the manually-tuned albedo parameters. This is most likely because their optimisation overfits  
699 the albedo retrievals without applying constraints to the other processes strongly impacting the SMB components  
700 and controlling the state of the snowpack (e.g., snow compaction, snow density, snow viscosity). This underlines  
701 the need for improving the representation of some internal processes and supports the recommendation for a multi-  
702 objective optimisation using not only albedo data, but also vertical temperature and density profiles as well as  
703 SMB observations. Since this type of approach is highly time-consuming, it has not yet been undertaken.  
704 Nevertheless, it will be the focus of a future study.  
705 A second potential limitation is related to missing processes. For example, metamorphism, dust and algae  
706 deposition that strongly affect the albedo, or snow drift, are ignored. In addition, there are also structural  
707 deficiencies related to the fact that in ORCHIDEE-ICE, a single energy budget is computed in one grid cell. This  
708 is detrimental for the albedo computation especially at the edges of the ice sheet where several surface types may  
709 coexist in a 20 km x 20 km mesh. However, the implementation of a multi-tile energy balance is currently under  
710 development.  
711 Finally, as our simulations have been run in off-line mode, the snow feedback onto the atmosphere has not been  
712 taken into account, contrary to the MAR model fully coupled to a snow scheme derived from CROCUS (Brun,  
713 1989, 1992). Ignoring snow-atmosphere feedback may potentially lead to biases related to surface processes and  
714 to an improper representation of the energy and humidity flux exchanges at the snow-atmosphere interface. For



715 example, forcing our model with the atmospheric temperature at 2m derived from the full coupled MAR simulation  
716 could lead to an underestimation of the energy available at the snow-atmosphere interface, resulting in less  
717 snowmelt compared to what is simulated in coupled mode. However, our manual tuning approach aims at limiting  
718 the potential underestimation of the surface meltwater production. Conversely, any potential bias in the MAR  
719 forcing may also affect our results (Dietrich et al., 2024). To overcome this problem, it would have been interesting  
720 to force ORCHIDEE-ICE by meteorological fields recorded at the automatic weather stations. This has not been  
721 done in this study because the meteorological fields required to force ORCHIDEE-ICE were not all available at  
722 the PROMICE stations and because our first objective was to obtain a reasonable estimate of the SMB and its  
723 components at the scale of the entire GrIS.

724 Despite the potential improvements that could still be made to ORCHIDEE-ICE to enhance the model's  
725 performance, the developments presented in this paper represent a major step forward. Indeed, they now allow the  
726 ice-sheet surfaces to be handled by the land surface model, consistently with all the other surface types, and not  
727 by the atmospheric component of the IPSL model (LMDZ), as was the case up to now. In addition, the new snow  
728 model can now be applied to the continental glaciers replacing the very crude snow scheme used previously. Our  
729 developments enable us to provide a reasonable estimate of the surface mass balance of the Greenland ice sheet,  
730 in very good agreement with that simulated by the MAR model which was used as a reference in this study. These  
731 developments constitute a first step towards the full coupling between the IPSL global climate model and ice-sheet  
732 models.

733



734 **Appendix A:**

735 **Table A1:** List of variables used in ORCHIDEE-ICE and related to snowpack and ice processes

| Symbol               | Variable  | Units             | Value/Range |
|----------------------|---|-------------------|-------------|
| $dt$                 | ORCHIDEE time step  | s                 | 1800        |
| $G_{surf}$           | Surface energy flux   | $W m^{-2}$        |             |
| $G_{freezing}$       | Surface energy flux over snow-covered areas                     | $W m^{-2}$        |             |
| $SW_{net}$           | Shortwave net radiation   | $W m^{-2}$        |             |
| $LW_{net}$           | Longwave net radiation  | $W m^{-2}$        |             |
| $H_L$                | Latent heat flux  | $W m^{-2}$        |             |
| $H_S$                | Sensible heat flux  | $W m^{-2}$        |             |
| $H_{rainfall}$       | Heat release from rainfall                                      | $W m^{-2}$        |             |
| $C_{soil}$           | Surface heat capacity of soil                                   | $J m^{-2} K^{-1}$ |             |
| $F_C$                | Heat conductive flux  | $W m^{-2}$        |             |
| $q_{cdrag}$          | Transfer coefficient  | -                 |             |
| $U$                  | Wind speed at 10 m  | $m s^{-1}$        |             |
| $F_{snow}$           | Snow cover fraction   | -                 |             |
| $z_{og}$             | Ground roughness length   | m                 | 0.01        |
| $m$                  | Adjustable parameter in the snow cover fraction formulation     |                   | 1.0         |
| $\alpha$             | Surface albedo of the grid cell                                 |                   |             |
| $\alpha_{snow}$      | Albedo of snow-covered surfaces                                 |                   |             |
| $\alpha_{snow-free}$ | Albedo of snow-free surfaces                                    |                   |             |
| $f_{ice}$            | Grid-cell fraction of ice-covered areas                         |                   |             |
| $f_{PFT,i}$          | Grid-cell fraction of the $i^{th}$ PFT                          |                   |             |
| $A_{aged}$           | Snow albedo of old snow   |                   |             |
| $A_{aged} + B_{dec}$ | Albedo of fresh snow  |                   |             |
| $\tau_{snow}$        | Snow age  | days              |             |
| $\tau_{dec}$         | Time constant of the albedo decay                               | days              |             |
| $\tau_{max}$         | Maximum snow age  | days              |             |
| $\delta_c$           | Snowfall thickness necessary for resetting the snow age to zero | m                 |             |
| $\omega_1, \omega_2$ | Tuning constants for snow albedo                                |                   |             |



|                       |  |                                    |                        |
|-----------------------|--|------------------------------------|------------------------|
| $\alpha_{ice}$        | Ice albedo   |                                    |                        |
| $f_{age}$             | Snow age function  |                                    |                        |
| $T_{air}$             | Surface air temperature at 2 m   | K                                  |                        |
| $\rho_{air}$          | Air density  | kg m <sup>-3</sup>                 |                        |
| $Q_{air}$             | Air specific humidity at 2 m   | -                                  |                        |
| $Q_{sat}$             | Saturated specific humidity at 2 m   | -                                  |                        |
| $P$                   | Atmospheric pressure   | hPa                                |                        |
| $P_0$                 | Reference pressure   | hPa                                | 1000                   |
| $L_s$                 | Latent heat of sublimation   | J kg <sup>-1</sup>                 | 2.8345 10 <sup>6</sup> |
| $T_{surf}$            | Surface temperature  | K                                  |                        |
| $T_0$                 | Freezing temperature   | K                                  | 273.15                 |
| $T_{snow}^{add}$      | Snow temperature adjustment  | K                                  |                        |
| $T_{snow} (T_{ice})$  | Snow (ice) temperature   | K                                  |                        |
| $P_{snow}$            | Snowfall amount during the time step dt                                    | m                                  |                        |
| $P_{rain}$            | Liquid precipitation during the time step dt                               | m                                  |                        |
| $S_{snow}$            | Snow sublimation   | kg m <sup>-2</sup> s <sup>-1</sup> |                        |
| $C_{snow}$            | Snow heat capacity   | J m <sup>-2</sup> K <sup>-1</sup>  |                        |
| $C_{snow}^v, C_{ice}$ | Snow (ice) volumetric heat capacity  | J m <sup>-3</sup> K <sup>-1</sup>  |                        |
| $Z_{snow}$            | Total snow depth   | m                                  |                        |
| $Z_{thin}$            | Minimum thickness of the snowpack  | m                                  | 0.1                    |
| $\rho_{snow}$         | Snow density   | kg m <sup>-3</sup>                 |                        |
| $H_{snow}^i$          | Heat content in the i <sup>th</sup> snow layer                             | W m <sup>-2</sup> s <sup>-1</sup>  |                        |
| $D_{snow}^i$          | Depth of the i <sup>th</sup> snow layer                                    | m                                  |                        |
| $\delta_i$            | Maximum thickness of the i <sup>th</sup> layers for i = 1 to 5 and 9 to 12 | m                                  |                        |
| $d_r$                 | Total thickness of layers 6 to 8   | m                                  |                        |
| $\sigma_{snow}^i$     | Pressure of the snow load over the i <sup>th</sup> layer                   | Pa                                 |                        |
| $W_{liq}^i$           | Liquid content in the i <sup>th</sup> snow layer                           | m                                  |                        |
| $D_{swe}^i$           | Snow water equivalent in the i <sup>th</sup> snow layer                    | m                                  |                        |
| $W_{max}^i$           | Maximum water holding capacity of the i <sup>th</sup> snow layer           | m                                  |                        |
| $r_{min}$             | Parameter of the maximum water holding capacity                            |                                    | 0.03                   |



|                                  |  |   |                                  |
|----------------------------------|--|---|----------------------------------|
| $r_{max}$                        | Parameter of the maximum water holding capacity                      |   | 0.10                             |
| $\rho_t$                         | Parameter of the maximum water holding capacity                      | $\text{kg m}^{-3}$                          | 200                              |
| $\eta_{snow}$                    | Snow viscosity   | $\text{Pa s}$                               |                                  |
| $\eta_0$                         | Snow viscosity parameter   | $\text{Pa s}$                               | $3.7 \times 10^7$                |
| $a_\eta$                         | Snow viscosity parameter   | $\text{K}^{-1}$                             | $8.1 \times 10^{-2}$             |
| $b_\eta$                         | Snow viscosity parameter   | $\text{m}^3 \text{kg}^{-1}$                 | $1.8 \times 10^{-2}$             |
| $a_\psi$                         | Parameter for the effect of metamorphism                             | $\text{s}^{-1}$                             | $2.8 \times 10^{-6}$             |
| $b_\psi$                         | Parameter for the effect of metamorphism                             | $\text{K}^{-1}$                             | $4.2 \times 10^{-2}$             |
| $c_\psi$                         | Parameter for the effect of metamorphism                             | $\text{m}^3 \text{kg}^{-1}$                 | $460 \text{ m}^3 \text{kg}^{-1}$ |
| $\rho_\psi$                      | Parameter for the effect of metamorphism                             | $\text{kg m}^{-3}$                          | 150                              |
| $\Lambda_{snow} (\Lambda_{ice})$ | Snow (ice) thermal conductivity                                      | $\text{W m}^{-1} \text{K}^{-1}$             |                                  |
| $\Lambda_{eff} = \Lambda_{snow}$ | Effective snow thermal conductivity                                  | $\text{W m}^{-1} \text{K}^{-1}$             |                                  |
| $\Lambda_{cond}$                 | Snow thermal conductivity  | $\text{W m}^{-1} \text{K}^{-1}$             |                                  |
| $\Lambda_{vap}$                  | Snow thermal conductivity  | $\text{W m}^{-1} \text{K}^{-1}$             |                                  |
| $\rho_{ice}$                     | Ice density  | $\text{kg m}^{-3}$                          | 920                              |
| $D_{ice}^i$                      | Depth of the $i^{\text{th}}$ ice layer                               | $\text{m}$                                  |                                  |
| $a_\lambda$                      | Parameter of snow thermal conductivity                               | $\text{W m}^{-1} \text{K}^{-1}$             | 0.02                             |
| $b_\lambda$                      | Parameter of snow thermal conductivity                               | $\text{W m}^5 \text{K}^{-1} \text{kg}^{-2}$ | $2.5 \cdot 10^{-6}$              |
| $a_{\lambda v}$                  | Parameter of snow thermal conductivity from vapor transport          | $\text{W m}^{-1} \text{K}^{-1}$             | -0.06023                         |
| $b_{\lambda v}$                  | Parameter of snow thermal conductivity from vapor transport          | $\text{W m}^{-1}$                           | -2.5425                          |
| $c_{\lambda v}$                  | Parameter of snow thermal conductivity from vapor transport          | $\text{K}$                                  | -289.99                          |
| $a_{ci}$                         | Parameter of heat capacity of the ice                                | $\text{J K}^{-1} \text{kg}^{-1}$            | 2115.3                           |
| $b_{ci}$                         | Parameter of heat capacity of the ice                                | $\text{J K}^{-2} \text{kg}^{-1}$            | 7.79293                          |
| $a_{\lambda i}$                  | Parameter of ice thermal conductivity                                | $\text{W m}^{-1} \text{K}^{-1}$             | 6.627                            |
| $b_{\lambda i}$                  | Parameter of ice thermal conductivity                                | $\text{K}^{-1}$                             | -0.041                           |
| $\rho_{water}$                   | Water density  | $\text{Kg m}^{-3}$                          | 1000                             |
| $E_{snow}^i (E_{ice}^i)$         | Energy required to induce phase changes in the snowpack (in the ice) | $\text{W m}^{-2} \text{s}^{-1}$             |                                  |



|  |   |                     |
|--|---|---------------------|
| $S_{melt} (I_{melt})$                        | Total amount of snow (ice) melt at each time step                 | kg m <sup>-2</sup>  |
| $\lambda_{snow}, C_{gr\_snow}, D_{gr\_snow}$ | Integration coefficient for snow thermal profile numerical scheme |                     |
| $\lambda_{ice}, C_{gr\_ice}, D_{gr\_ice}$    | Integration coefficient for ice thermal profile numerical scheme  |                     |
| $SMB$  | Surface mass balance  | Gt yr <sup>-1</sup> |

736

737 **Code availability:** The source code for the ORCHIDEE-ICE version used in this study is freely available online  
738 via the following address <https://doi.org/10.14768/d82899b4-09b4-4337-abb1-75886602fe72> (IPSL Data  
739 Catalogue, 2024). The ORCHIDEE model code is written in Fortran 90 and is maintained and developed under a  
740 subversion (SVN) control system at the Institut Pierre Simon Laplace (IPSL) in France.

741 **Data availability:** The MAR outputs are available at <ftp://ftp.climato.be/fettweis> (last access 30 October 2020).  
742 The MODIS Greenland albedo retrievals MOD10A1 are available at <https://doi.org/10.22008/FK2/6JAOPK> (last  
743 access 22 January 2024, Box et al., 2022).

744 **Author contributions:** SC conceived the project funding the study. SC, CD, FM and CO co-designed the research  
745 and contributed to the code developments. SC and CD performed the preliminary tests with strong support from  
746 FM and CO. CD implemented the new snow-layering scheme and the new icy soil type. XF ran the MARv3.11.4  
747 simulations and provided the MAR outputs. NR provided the albedo parameters obtained from the data  
748 assimilation experiment. SC, CD, FM and CO analysed the results with contributions from NR and XF. SC wrote  
749 the original draft, with contributions from CD, FM and CO, and generated the figures. All co-authors provided  
750 comments on the manuscript.

751 **Competing interests:** The authors declare that one of the co-authors is a member of the editorial board of *The*  
752 *Cryosphere*.

753 **Acknowledgements:** This work has been funded by the French INSU/LEFE OSCAR project. The authors would  
754 like to thank all members of the SNOW working group gathering members from the Institut Pierre Simon Laplace  
755 (IPSL, France) and the Institut des Géosciences de l'Environnement (IGE, France) for numerous and fruitful  
756 discussions. They also thank the core ORCHIDEE team for maintaining the model and especially J. Ghattas for  
757 helping merge the ORCHIDEE-ICE code into the trunk version of the model. Data from the Programme for  
758 Monitoring of the Greenland Ice Sheet (PROMICE) are provided by the Geological Survey of Denmark and  
759 Greenland (GEUS) at <http://www.promice.dk>. They include sites financially supported by the Glaciobasis  
760 programme as part of Greenland Ecosystem Monitoring (<https://g-e-m.dk/>), maintained by GEUS (ZAK, LYN)  
761 and by Asiaq Greenland Survey (NUK\_K). The WEG stations are paid for and maintained by the University of  
762 Graz.

## 763 References

- 764 Alexander, P. M., Tedesco, M., Fettweis, X., van de Wal, R. S. W., Smeets, C. J. P. P., and van den Broeke, M.  
765 R.: Assessing spatio-temporal variability and trends in modelled and measured Greenland Ice Sheet albedo (2000–  
766 2013), *The Cryosphere*, 8, 2293–2312, doi: [org/10.5194/tc-8-2293-2014](https://doi.org/10.5194/tc-8-2293-2014), 2014.
- 767 Armstrong, R. L. and Brun, E.: *Snow and Climate: Physical processes, surface energy exchange and modeling*,  
768 Cambridge University Press, 222p., 2008.
- 769 Anderson, E. A.: A point energy and mass balance model of a snow cover, Technical Report NWS 19, National  
770 Oceanic and Atmospheric Administration (NOAA), Silver Spring, MD, USA, 150pp., 1976.



- 771 Bakker, P, Schmittner, A., Lenaerts, J. T. M., Abe-Ouchi, A., Bi, D., van den Broecke, M. R., Chan, W. L., Hu,  
772 A., Beadling, R. L., Marsland, S. J., Mernild, S. H., Saenko, O. A., Swingedouw, D., Sullivan, A. and Yin, J.: Fate  
773 of the Atlantic Meridional Overturning Circulation: Strong decline under continued warming and Greenland  
774 melting, *Geophysical Research Letters*, 43, 12,252–12,260, doi:10.1002/2016GL070457, 2016.
- 775 Bennartz, R., Shupe, M. D., Turner, D.D., Walden, V. P., Steffen, K., Cox, C. J., Kulie, M. S., Miller, N. B. and  
776 Pettersen, C.: July 2012 Greenland melt extent enhanced by low-level liquid clouds, *Nature* 496, 83-86, doi:  
777 10.1038/nature120002, 2013.
- 778 Bonelli, S., Charbit, S., Kageyama, M., Woillez, M.-N., Ramstein, G., Dumas, C. and Quiquet A.: Investigating  
779 the evolution of major Northern Hemisphere ice sheets during the last glacial cycle, *Climate of the Past*, 5, 329-  
780 245, doi: 10.5194/cp-5-329-2009, 2009.
- 781 Boone, A., and Etchevers, P.: An intercomparison of three snow schemes of varying complexity coupled to the  
782 same land surface model: Local-scale evaluation at an Alpine site. *Journal of Hydrometeorology*, 2(4), 374-394,  
783 2001.
- 784 Boucher, O., Servonnat, J., Albright, A. L., Aumont, O., Balkanski, Y., Bastrikov, V., et al.: Presentation and  
785 evaluation of the IPSL-CM6A-LR climate model, *Journal of Advances in Modeling Earth Systems*, 12,  
786 e2019MS002010, doi: 10.1029/2019MS002010, 2020.
- 787 Bougamont, M., Bamber, J. L., Ridley, J. K., Gladstone, R. M., Greuell, W., Hanna, E., Payne, A. J and Rutt, I.:  
788 Impact of model physics on estimating the surface mass balance of the Greenland ice sheet, *Geophysical Research*  
789 *Letters*, 34, L17501, doi:10.1029/2007GL030700, 2007.
- 790 Born, A., Imhof, M. A., and Stocker, T. F.: An efficient surface energy-mass balance model for snow and ice, *The*  
791 *Cryosphere*, 13, 1529-1546, doi: 10.5194/tc-13-1529-2019, 2019.
- 792 Box, J. E., Fettweis, X., Stroeve, J. C., Tedesco, M., Hall, D. K., and Steffen, K.: Greenland ice sheet albedo  
793 feedback: thermodynamics and atmospheric feedbacks, *The Cryosphere*, 6, 821-839, doi: 10.5194/tc-821-2012,  
794 2012.
- 795 Box, J. E., van As, D., and Steffen, K.: Greenland, Canadian and Icelandic land-ice albedo grids (2000–2016),  
796 *GEUS Bulletin*, 38, 53–56, doi: 10.34194/geusb.v38.4414, 2017.
- 797 Brun, E., Martin, E., Simon, V., Gendre, C. and Coleou, C.: An energy and mass model of snow cover suitable for  
798 operational avalanche forecasting, *Journal of Glaciology*, 35 (121), 333-342, doi: 10.3189/S0022143000009254,  
799 1989.
- 800 Brun, E., David, P., Sudul, M., and Brunot, G.: A numerical model to simulate snow cover stratigraphy for  
801 operational avalanche forecasting, *Journal of Glaciology*, 38 (128), 13–22, doi: 10.3189/S0022143000009552,  
802 1992.
- 803 Chalita, S. and Le Treut, H.: The albedo of temperate and boreal forest and the Northern Hemisphere climate: a  
804 sensitivity experiment using the LMD GCM, *Climate Dynamics*, 10, 231-240, doi: 10.1007/BF00208990, 1994.
- 805 Charbit, S., Kageyama, M., Roche, D., Ritz, C; and Ramstein, G.: Investigating the mechanisms leading to the  
806 deglaciation of past continental Northern hemisphere ice sheets with the CLIMBER-GREMLINS coupled model,  
807 *Global and Planetary changes*, 48, 253-273, doi: 10.1016/j.gloplacha.2005.01.002, 2005.
- 808 Charbit, S., D. Paillard, and G. Ramstein (2008), Amount of CO2 emissions irreversibly leading to the total melting  
809 of Greenland, *Geophysical Research Letters*, 35, L12503, doi:10.1029/2008GL033472, 2008.





- 810 Charbit, S., Dumas, C., Kageyama, M., Roche, D. M. and Ritz, C.: Influence of ablation-related processes in the  
811 build-up of Northern Hemisphere ice sheets during the last glacial cycle, *The Cryosphere*, 7, 681-698, doi:  
812 10.5194/tc-7-681-2013, 2013.
- 813 Cheruy, F., Ducharne, A., Hourdin, F., Musat, I., Vignon, É., Gastineau, G., et al.: Improved near-surface  
814 continental climate in IPSL-CM6A-LR by combined evolutions of atmospheric and land surface physics, *Journal*  
815 *of Advances in Modeling Earth Systems*, 12, e2019MS002005., doi: 10.1029/2019MS002005, 2020.
- 816 Cristea, N. C., Bennett, A., Nijssen, B. and Lundquist, J. D.: When and where are multiple snow layers important  
817 for simulations of snow accumulation and melt? *Water Resources Research*, 58, e2020WR028993, doi:  
818 10.1029/2020WR028993, 2022.
- 819 Cullather, R.I., Nowicki, S.M.J., Zhao, B. and Suarez, M.J.: Evaluation of the Surface Representation of the  
820 Greenland Ice Sheet in a General Circulation Model, *Journal of Climate*, 27(13), 4835–4856, doi:10.1175/jcli-d-  
821 13-00635.1, 2014.
- 822 Decharme, B., Brun, E., Boone, A., Delire, C., Le Moigne, P. and Morin., S.: Impacts of snow and organic soils  
823 parameterization on northern Eurasian soil temperature profiles simulated by the ISBA land surface model, *The*  
824 *Cryosphere*, 10, 853\_877, doi: 10.5194/tc-10-853-2016, 2016.
- 825 Dee, D. P., Uppala, S. M., Simmons, A. J., Berrisford, P., Poli, P., Kobayashi, S., Andrae, U., Balmaseda, M.A.,  
826 Balsamo, G., Bauer, P., Bechtold, P., Beljaars, A., C., M., van de Berg, L., Bidlot, J., Bormann, N., Delsol, C.,  
827 Dragani, R., Fuentes, M., Geer, A.J., Haimberger, L., Healy, S. B., Hersbach, H., Hólm, E.V., Isaksen, L., Kallberg,  
828 P., Köhler, M., Matricardi, M., McNally, A.P., Monge-Sanz, B. M., Morcrette, J.-J., Park, B.-K., Peubey, C., de  
829 Rosnay, P., Tavolato, C., Thépaut, J.-N. and Vitart, F.: The ERA-Interim reanalysis: configuration and  
830 performance of the data assimilation system. *Quarterly Journal of the Royal Meteorological Society*, 137, 553–597,  
831 doi:10.1002/qj.828, 2011.
- 832 Delhasse, A., Kittel, C., Amory, C., Hofer, S., van As, D., S. Fausto, R., and Fettweis, X.: Brief communication:  
833 Evaluation of the near-surface climate in ERA5 over the Greenland Ice Sheet, *The Cryosphere*, 14, 957–965,  
834 doi:10.5194/tc-14-957-2020, 2020.
- 835 Dietrich, L. J., Steen-Larsen, H. C., Wahl, S., Faber, A.-K., and Fettweis, X.: On the importance of the humidity  
836 flux for the surface mass balance in the accumulation zone of the Greenland Ice Sheet, *The Cryosphere*, 18, 289–  
837 305, doi: 10.5194/tc-18-289-2024, 2024.
- 838 Dutra, E., Balsamo, E., Viterbo, P., Miranda, P. M. A., Beljaars, A., Schär, C. and Elder, K.: An Improved Snow  
839 Scheme for the ECMWF Land Surface Model: Description and Offline Validation, *Journal of Hydrometeorology*,  
840 11(4); 899-916, doi: 10.1175/2010JHM1249.1, 2010.
- 841 Edwards, T. L., Fettweis, X., Gagliardini, O., Gillet-Chaulet, F., Goelzer, H., Gregory, J. M., Hoffman, M.,  
842 Huybrechts, P., Payne, A.J., Perego, M., Price, S., Quiquet, A. and Ritz, C.: Effect of uncertainty in surface mass  
843 balance–elevation feedback on projections of the future sea level contribution of the Greenland ice sheet, *The*  
844 *Cryosphere*, 8, 195-208, doi: 10.5194/tc-8-195-2014, 2014.
- 845 Enderlin, E. M., Howat, I. M., Jeong, S. Noh, M.-J., van Angelen, J. H. and van den Broeke, M. R. An improved  
846 mass budget for the Greenland ice sheet, *Geophysical Research Letters*, 41, 866–872,  
847 doi:10.1002/2013GL059010, 2014.



848 Eyring, V., Bony, S. Meehl, G. A. Senior, C. A., Stevens, B., Stouffer, R. and Taylor, K. E.: Overview of the  
849 Coupled Model Intercomparison Project Phase 6 (CMIP6) experimental design and organization, *Geoscientific*  
850 *Model Development*, 9, 1937-1958, doi: 10.5194/gmd-9-1937-2016, 2016.

851 Fausto, R. S., van As, D., Mankoff, K. D., Vandecrux, B., Citterio, M., Ahlstrøm, A. P., et al.: Programme for  
852 Monitoring of the Greenland Ice Sheet (PROMICE) automatic weather station data, *Earth System Scientific Data*,  
853 13, 3819-3845, doi: 10.5194/essd-13-3819-2021, 2021.

854 Fettweis, X., Box, J. E., Agosta, C., Amory, C., Kittel, C., Lang, C., van As, D., Machguth, H., and Gallée, H.:  
855 Reconstructions of the 1900–2015 Greenland ice sheet surface mass balance using the regional climate MAR  
856 model, *The Cryosphere*, 11, 1015–1033, <https://doi.org/10.5194/tc-11-1015-2017>, 2017.

857 Fettweis, X. Hofer, S., Krebs-Kanzow, U., Amory, C., Aoki, T., Berends, C. J., et al.: GrSMBMIP:  
858 Intercomparison of the modelled 1980-2012 surface mass balance over the Greenland Ice sheet, *The Cryosphere*,  
859 14, 3935-3958, doi: 10.5194/tc-14-3935-2020, 2020.

860 Franco, B., Fettweis, X., Lang, C., and Ericpicum, M.: Impact of spatial resolution on the modelling of the Greenland  
861 ice sheet surface mass balance between 1990–2010, using the regional climate model MAR, *The Cryosphere*, 6,  
862 695–711, doi: 10.5194/tc-6-695-2012, 2012.

863 Fox-Kemper, B., H.T. Hewitt, C. Xiao, G. Aðalgeirsdóttir, S.S. Drijfhout, T.L. Edwards, N.R. Golledge, M.  
864 Hemer, R.E. Kopp, G. Krinner, A. Mix, D. Notz, S. Nowicki, I.S. Nurhati, L. Ruiz, J.-B. Sallée, A.B.A. Slangen,  
865 and Y. Yu: Ocean, Cryosphere and Sea Level Change. *In Climate Change 2021: The Physical Science Basis.*  
866 *Contribution of Working Group I to the Sixth Assessment Report of the Intergovernmental Panel on Climate*  
867 *Change [Masson-Delmotte, V., P. Zhai, A. Pirani, S.L. Connors, C. Péan, S. Berger, N. Caud, Y. Chen, L.*  
868 *Goldfarb, M.I. Gomis, M. Huang, K. Leitzell, E. Lonnoy, J.B.R. Matthews, T.K. Maycock, T. Waterfield, O.*  
869 *Yelekçi, R. Yu, and B. Zhou (eds.)]. Cambridge University Press, Cambridge, United Kingdom and New York,*  
870 *NY, USA, pp. 1211–1362, doi:10.1017/9781009157896.011, 2021.*

871 Fyke, J., Sergienko, O., Löfverström, M., Price, S. and Lenaerts, J. T., M.: An overview of interactions and  
872 feedbacks between ice sheets and the Earth system, *Review of Geophysics*, 56, doi: 10.1029/2018GR000600,  
873 2018.

874 Gallée, H. and Schayes, G.: Development of a three-dimensional meso-primitive equations model: Katabatic winds  
875 simulation in the area of Terra Nova Bay, Antarctica, *Monthly Weather Review*, 122, 671–685, doi: 10.1175/1520-  
876 0493(1994)122%3C0671:DOATDM%3E2.0.CO;2, 1994.

877 Hahn, L. C., Storelvmo, T., Hofer, S., Parfitt, R. and Ummenhofer, C. C.: Importance of orography for Greenland  
878 ice sheet cloud and melt response to atmospheric blocking, *Journal of Climate*, 33, 4187-4206, doi: 10.1175/JCLI-  
879 D-19\_0527.1, 2020.

880 Hall, D. and Riggs, G.: MODIS/Terra Snow Cover Daily L3 Global 500m Grid, Version 6. Greenland coverage.,  
881 National Snow and Ice Data Center, NASA Distributed Active Archive Center, Boulder, Colorado USA.,  
882 <http://nsidc.org/data/MOD10A1/versions/6>, accessed December 2016., 2016.

883 Hall, D. K., Riggs, G. A., and Salomonson, V. V.: Development of methods for mapping global snow cover using  
884 moderate resolution imaging spectroradiometer data, *Remote sensing of Environment*, 54, 127–140, doi:  
885 10.1016/0034-4257(95)00137-P, 1995, 1995.



- 886 Helsen, M. M., van de Wal, R. S. W., Reerink, T. J., Bintanja, R., Madsen, M. S., Yang, S., Li, Q., and Zhang, Q.:  
887 On the importance of the albedo parameterization for the mass balance of the Greenland ice sheet in EC-Earth,  
888 *The Cryosphere*, 11, 1949–1965, doi: 10.5194/tc-11-1949-2017, 2017.
- 889 Hersbach, H., Bell, B., Berrisford, P., Hirahara, S., Horányi, A., Muñoz-Sabater, J., Nicolas, J., Peubey, C., Radu,  
890 R., Schepers, D., Simmons, A., Soci, C., Abdalla, S., Abellan, X., Balsamo, G., Bechtold, P., Biavati, G., Bidlot,  
891 J., Bonavita, M., De Chiara, G., Dahlgren, P., Dee, D., Diamantakis, M., Dragani, R., Flemming, J., Forbes, R.,  
892 Fuentes, M., Geer, A., Haimberger, L., Healy, S., Hogan, R.J., Hólm, E., Janisková, M., Keeley, S., Laloyaux, P.,  
893 Lopez, P., Lupu, C., Radnoti, G., de Rosnay, P., Rozum, I., Vamborg, F., Villaume, S. and Thépaut, J.-N.: The  
894 ERA5 global reanalysis. *Quarterly Journal of the Royal Meteorological Society*, 146, 1999–2049. doi:  
895 10.1002/qj.3803, 2020.
- 896 Kageyama, M., Charbit, S., Ritz, C., Khodri, M. and Ramstein G.: Quantifying ice-sheet feedbacks during the last  
897 glacial inception, *Geophysical Research Letters*, 31, L24203, doi:10.1029/2004GL021339, 2004.
- 898 Kojima, K.: Densification of seasonal snow cover. *Physics of Snow and Ice: Proceedings of the International  
899 Conference on Low Temperature Science, Part 1, Sapporo, Japan, Hokkaido University*, 1 (2), 929–952, 1967.
- 900 Krinner, G., Viovy, N., de Noblet-Ducoudré, N., Ogée, J., Polcher, J., Friedlingstein, P., Ciais, P., Sitch, S., and  
901 Prentice, I. C.: A dynamic global vegetation model for studies of the coupled atmosphere-biosphere system, *Global  
902 Biogeochemical Cycles*, 19, GB1015, doi:10.1029/2003GB002199, 2005.
- 903 Lefebre, F., Gallée, H., van Ypersele, J.-P. and W. Greuell, Modeling of snow and ice melt at ETH Camp (West  
904 Greenland): A study of surface albedo, *Journal of Geophysical Research*, 108(D8), 4231,  
905 doi:10.1029/2001JD001160, 2003.
- 906 Louis, J. F.: A parametric model of vertical eddy fluxes in the atmosphere. *Boundary-Layer Meteorology*, 17(2),  
907 187-202, 1979.
- 908 Lynch-Stieglitz, M.: The development and validation of a simple snow model for the GISS GCM, *Journal of  
909 Climate*, 7, 1842-1855, doi: 10.1175/1520-0442(1994)007%3C1842:TDAVOA%3E2.0.CO;21994, 1994.
- 910 Martin, T., Biastoch, A., Lohmann, G., Mikolajewicz, U., and Wang, X.: On timescales and reversibility of the  
911 ocean's response to enhanced Greenland Ice Sheet melting in comprehensive climate models. *Geophysical  
912 Research Letters*, 49, e2021GL097114. doi: 10.1029/2021GL097114, 2022.
- 913 Mellor, M.: Snow and Ice on the Earth's Surface, *Cold regions science and engineering. Part 2, Physical science.  
914 Sect. C, The physics and mechanics of ice Snow and Ice on the Earth's Surface*, U.S. Army Materiel Command,  
915 Cold Regions Research and Engineering Laboratory, 163pp., 1964.
- 916 Monin, A. S., and Obukhov, A. M.: Basic laws of turbulent mixing in the surface layer of the atmosphere. *Contrib.  
917 Geophys. Inst. Acad. Sci. USSR*, 151(163), e187, 1954.
- 918 Montgomery L, Koenig L, Lenaerts JTM, Kuipers Munneke P (2020). Accumulation rates (2009–2017) in  
919 Southeast Greenland derived from airborne snow radar and comparison with regional climate models. *Annals of  
920 Glaciology* 61(81), 225–233, doi: 10.1017/aog.2020.8, 2020.
- 921 Muntjewerf, L., Sellevod, R., Vizcaino, M., Ernani da Silva, C., Petrini, M., Thayer-Calder, K., Scherrenberg, M.  
922 D. W., Bradley; S. L., Katsman, C. A., Fyke, J., Lipscomb, W. H., Löffverström, M. and Sacks, W.J.: Accelerated  
923 Greenland ice sheet mass loss under high greenhouse gas forcing as simulated by the coupled CESM2.1-CISM2.1,  
924 *Journal of Advances Modeling in Earth Systems*, 12, e2019MS002031, doi: 10.1029/2019MS002031, 2020.



- 925 Niu, G.-Y., and Yang, Z.-L.: An observation-based formulation of snow cover fraction and its evaluation over  
926 large North American river basins, *Journal of Geophysical Research*, 112, D21101, doi:10.1029/2007JD008674,  
927 2007.
- 928 Noël, B., van de Berg, W. J., van Wessem, J. M., van Meijgaard, E., van As, D., Lenaerts, J. T. M. Lhermitte, S.,  
929 Kuipers Munneke, P., Smeets, C. J. P. P., van Ulft, L.H., van de Wal, R. S. W., and van den Broeke, M. R.:  
930 Modelling the climate and surface mass balance of polar ice sheets using RACMO2 – Part 1: Greenland (1958–  
931 2016), *The Cryosphere*, 12, 811–831, <https://doi.org/10.5194/tc-12-811-2018>, 2018.
- 932 Pahaut, E.: *La métamorphose des cristaux de neige (Snow crystal metamorphosis)*, Monographies de la  
933 Météorologie Nationale, No. 96, Météo France, Direction de la météorologie nationale, France, 58pp., 1976.
- 934 Patterson, W. S. B., *The Physics of Glaciers*, Butterworth-Heinemann, 1994.
- 935 Punge, H. J., Gallée, H., Kageyama, M. and Krinner, G.: Modelling snow accumulation on Greenland in Eemian,  
936 glacial inception, and modern climates in a GCM, *Climate of the Past*, 8, 1801–1819, doi: 10.5194/cp-8-1801-  
937 2012, 2012, 2012.
- 938 Raoult, N., Charbit, S., Dumas, C., Maignan, F., Otlé, C., and Bastrikov, V.: Improving modelled albedo over the  
939 Greenland ice sheet through parameter optimisation and MODIS snow albedo retrievals, *The Cryosphere*, 17,  
940 2705–2724, <https://doi.org/10.5194/tc-17-2705-2023>, 2023.
- 941 Reeh, N.: Parameterization of melt rate and surface temperature on the Greenland ice sheet, *Polarforschung*, 5913,  
942 113-128, 1991.
- 943 Reynolds, C. A., Jackson, T. J., and Rawls, W. J.: Estimating soil water-holding capacities by linking the Food  
944 and Agriculture Organization soil map of the world with global pedon databases and continuous pedotransfer  
945 functions, *Water Resources Research*, 36, 3653–3662, doi: 10.1029/2000WR900130, 2000.
- 946 Ridley, J. K., Huybrechts, P., Gregory, J. M. and Lowe, J. A.: Elimination of the Greenland ice sheet in a high  
947 CO<sub>2</sub> climate, *Journal of Climate*, 18, 3409-3427, doi: 10.1175/JCLI3482.1, 2005.
- 948 Riihelä, A., King, M. D. and Anttila K.: The surface albedo of the Greenland ice sheet between 1982 and 2015  
949 from CLARA-A2 dataset and its relationship to the ice sheet’s surface mass balance, *The Cryosphere*, 13, 2597-  
950 2614, doi: 10.5194/tc-13-2597-2019, 2019.
- 951 Roche, D. M., Dumas, C., Bügelmayr, M., Charbit, S. and Ritz, C.: Adding a dynamical cryosphere to  
952 iLOVECLIM (version 1.0): coupling with the GRISLI ice-sheet model, *Geoscientific Model Development*, 7,  
953 1377-1394, doi: 10.5194/gmd-7-1377-2014, 2014.
- 954 Ryan, J.V., Smith, L. C., van As, D., Cooley, S. W., Cooper, M. G., Pitcher, L. H., and Hubbard, A.: Greenland  
955 Ice Sheet surface melt amplified by snowline migration and bare ice exposure, *Science Advances*, 5, eaav3738,  
956 doi: 10.1126/sciadv.aav3738, 2019.
- 957 Sellevod, R., van Kampenhout, L., Lenaerts, J. T. M., Noël, B., Lipscomb, W. H. and Vizcaino, M.: Surface mass  
958 balance downscaling through elevation classes in an Earth system model: application to the Greenland ice sheet,  
959 *The Cryosphere*, 13, 3193-3208, doi: 10.5194/tc-13-3193-2019, 2019.
- 960 Smith, R. S., Mathiot P., Siahaan, A., Lee, V., Cornford, S. L., Gregory, J. M., Payne, A. J., Jenkins, A., Holland,  
961 P., R., Ridley, J. K. and Jones, C. G.: Coupling the U.K. Earth System Model to dynamic models of the Greenland  
962 and Antarctic ice sheets, *Journal of Advances Modeling in Earth Systems*, 13, e2021MS002520, doi:  
963 10.1029/2021MS002520, 2021.



- 964 Smith, B. E., Medley, B., Fettweis, X., Sutterley, T., Alexander, P., Porter, D., and Tedesco, M.: Evaluating  
965 Greenland surface-mass-balance and firn-densification data using ICESat-2 altimetry, *The Cryosphere*, 17, 789–  
966 808, doi: 10.5194/tc-17-789-2023, 2023.
- 967 Sun, S., Jin, J. and Xue, Y.: A simple snow-atmosphere-soil transfer model, *Journal of Geophysical Research*, 104  
968 (D16), 19587-19597, doi: 10.1029/1999JD900305, 1999.
- 969 Taylor, K. E., Stouffer, R. J. and Meehl, G. A.: An overview of CMIP5 and the experiment design, *Bulletin of*  
970 *American Meteorological Society*, 93, 485-498, doi: 10.1175/BAMS-D-11-00094.1, 2012.
- 971 Tedesco, M. and Fettweis, X.: Unprecedented atmospheric conditions (1948–2019) drive the 2019 exceptional  
972 melting season over the Greenland ice sheet, *The Cryosphere*, 14, 1209–1223, [https://doi.org/10.5194/tc-14-1209-](https://doi.org/10.5194/tc-14-1209-2020)  
973 2020, 2020.
- 974 The IMBIE team: Mass balance of the Greenland ice sheet from 1992 to 2018, *Nature*, 579, 233-239, doi:  
975 10.1038/s41586-019-1855-2, 2020.
- 976 Uppala, S.M., Källberg, P.W., Simmons, A.J., Andrae, U., da Costa Bechtold, V., Fiorino, M., Gibson, J.K.,  
977 Haseler, J., Hernandez, A., Kelly, G.A., Li, X., Onogi, K., Saarinen, S., Sokka, N., Allan, R.P., Andersson, E.,  
978 Arpe, K., Balmaseda, M.A., Beljaars, A.C.M., van de Berg, L., Bidlot, J., Bormann, N., Caires, S., Chevallier, F.,  
979 Dethof, A., Dragosavac, M., Fisher, M., Fuentes, M., Hagemann, S., Hólm, E.V., Hoskins, B.J., Isaksen, L.,  
980 Janssen, P.A.E.M., Jenne, R., McNally, A.P., Mahfouf, J.-F., Morcrette, J.-J., Rayner, N.A., Saunders, R.W.,  
981 Simon, P., Sterl, A., Trenberth, K.E., Untch, A., Vasiljevic, D., Viterbo, P. and Woollen, J.: The ERA-40 re-  
982 analysis. *Quarterly Journal of the Royal Meteorological Society*, 131, 2961–3012, 2005.
- 983 Urraca, R., Lanconelli, C., Cappucci, F., Gobron, N.: Comparison of Long-Term Albedo Products against Spatially  
984 Representative Stations over Snow, *Remote Sensing* 14, 3745, [doi: 10.3390/rs14153745](https://doi.org/10.3390/rs14153745), 2022.
- 985 Urraca, R., Lanconelli, C., Cappucci, F., Gobron, N.: Assessing the fitness of satellite albedo products for  
986 monitoring snow albedo trends, *IEEE Transactions on geoscience and remote sensing*, 61, 4404817, doi:  
987 10.1109/TGRS2023.3281188, 2023.
- 988 van den Broeke, M., Bamber, J., Ettema, J., Rignot, E., Schrama, E., van de Berg, W. J., van Meijgaard, E.,  
989 Velicogna, I., Wouters, B.: Partitioning recent Greenland mass loss, *Science*, 326, 984-986, doi:  
990 10.1126/science1178276, 2009.
- 991 van den Broeke, M., Enderlin, E. M., Howat, I. M., Kuipers Munnneke, P., Noël, B. P. Y., van de Berg, W. J., van  
992 Meijgaard, E., Wouters, B.: On the recent contribution of the Greenland ice sheet to sea level change, *The*  
993 *Cryosphere*, 10, 1933-1946, doi: 10.5194/tc-10-1933-2016, 2016.
- 994 van de Wal, R., S., W.: Mass-balance modelling of the Greenland ice sheet: a comparison of an energy-balance  
995 and a degree-day model, *Annals of Glaciology*, 23, 36-45, 1996.
- 996 Vionnet, V. Brun, E., Morin, S., Boone, A., Faroux, S., Le Moigne, P., Martin, E. and Willemet J.-M.: The detailed  
997 snowpack scheme Crocus and its implementation in SURFEX v7.2, *Geoscientific Model Development*, 5, 773-  
998 791, doi: 10.5194/gmd-5-773-2012, 2012.
- 999 Vizcaino, M., Mikolajewicz, U., Jungclaus, J. and Schurgers, G.: Climate modification by future ice sheet changes  
1000 and consequences for ice sheet mass balance, *Climate Dynamics*, 34, 301-324, doi: 10.1007/s00382-009-0591-y,  
1001 2010.



- 1002 Vizcaino, M., Lipscomb, W. H., Sacks, W. J., van Angelen, J. H., Wouters, B. and van den Broeke, M. R.:  
1003 Greenland surface mass balance as simulated by the Community Earth System Model. Part I: Model evaluation  
1004 and 1850-2005 results, *Journal of Climate*, 26, 7793-7812, doi: 10.1175/JCLI-D-00615.1, 2013.
- 1005 Vizcaino, M.: Ice sheets as interactive components of Earth System Models: progress and challenges, *WIREs*  
1006 *Climate Change*, 5, 557–568. doi: 10.1002/wcc.285, 2014.
- 1007 Wang, T., Ottlé, C., Boone, A., Ciais, P., Brun, E., Morin, S., Krinner, G., Piao, S. and Peng, S.: Evaluation of an  
1008 improved intermediate complexity snow scheme in the ORCHIDEE land surface model, *Journal of Geophysical*  
1009 *Research Atmosphere*, 118, 6064–6079, doi:10.1002/jgrd.50395, 2013.
- 1010 Wang, T., Peng, S., Krinner, G., Ryder, J., Li, Y., Dantec-Nédélec, S. and Ottlé, C.: Impacts of Satellite-Based  
1011 Snow Albedo Assimilation on Offline and Coupled Land Surface Model Simulations. *PLoS ONE* 10(9): e0137275,  
1012 doi:10.1371/journal.pone.0137275, 2015.
- 1013 Yen, Y.-C.: Review of thermal properties of snow, ice and sea ice. *Cold Regions Research and Engineering*  
1014 *Laboratory*, Hanover, NH, 1981.